Cell Reports

Article

KDM6B-dependent chromatin remodeling underpins effective virus-specific CD8$^+$ T cell differentiation

Graphical Abstract

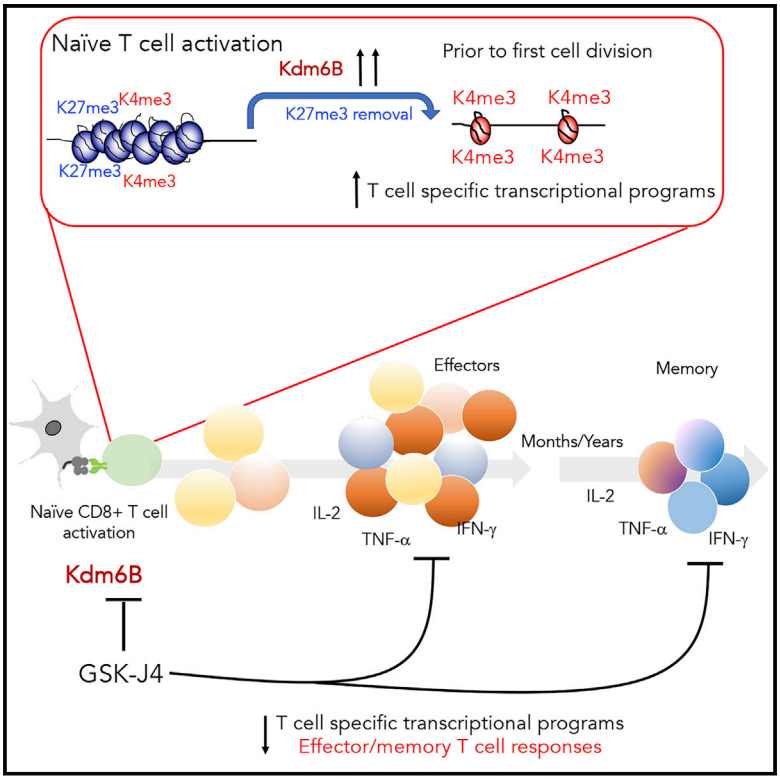

Highlights

- Naive CD8$^+$ T cell activation results in chromatin changes prior to first cell division
- The H3K27me3 demethylase KDM6B is rapidly upregulated upon T cell activation
- H3K27me3 demethylation occurs in a stepwise manner ensuring optimal T cell activation
- Perturbation of KDM6B function results in suboptimal virus-specific CD8$^+$ T cell memory

Authors

Jasmine Li, Kristine Hardy, Moshe Olshansky, ..., Paul J. Hertzog, Sudha Rao, Stephen J. Turner

Correspondence

stephen.j.turner@monash.edu

In brief

Li et al. demonstrate that naive CD8$^+$ T cell activation results in extensive KDM6B-dependent chromatin demethylation prior to first cell division. Inhibition of early chromatin demethylation resulted in dysregulated T cell activation and suboptimal virus-specific CD8$^+$ effector and memory T cell responses.

Li et al., 2021, Cell Reports *34*, 108839
March 16, 2021
https://doi.org/10.1016/j.celrep.2021.108839

CellPress

Cell Reports

CellPress
OPEN ACCESS

Article

KDM6B-dependent chromatin remodeling underpins effective virus-specific CD8$^+$ T cell differentiation

Jasmine Li,[1] Kristine Hardy,[2] Moshe Olshansky,[1,7] Adele Barugahare,[1] Linden J. Gearing,[3] Julia E. Prier,[4] Xavier Y.X. Sng,[5] Michelle Ly Thai Nguyen,[4,8] Dana Piovesan,[4] Brendan E. Russ,[1] Nicole L. La Gruta,[5] Paul J. Hertzog,[3] Sudha Rao,[6] and Stephen J. Turner[1,3,9,*]

[1]Department of Microbiology, Biomedicine Discovery Institute, Monash University, Clayton, VIC 3800, Australia
[2]Epigenetics and Transcription Laboratory Melanie Swan Memorial Translational Centre, Sci-Tech, University of Canberra, Bruce, ACT 2617, Australia
[3]Hudson Institute for Medical Research, Clayton, VIC 3168, Australia
[4]Department of Microbiology and Immunology, the Doherty Institute, University of Melbourne, Parkville, VIC 3010, Australia
[5]Department of Biochemistry and Molecular Biology, Biomedicine Discovery Institute, Monash University, Clayton, VIC 3800, Australia
[6]QIMR Berghofer Gene Regulation and Translational Medicine Laboratory, Department of Immunology, QIMR Berghofer Medical Research Institute, Brisbane, QLD, Australia
[7]Present address: Computational Biology & Bioinformatics, Baker Heart & Diabetes Institute, Melbourne, VIC 3004, Australia
[8]Present address: Department of Microbiology and Immunology, University of California, San Francisco, CA, USA
[9]Lead contact
*Correspondence: stephen.j.turner@monash.edu
https://doi.org/10.1016/j.celrep.2021.108839

SUMMARY

Naive CD8$^+$ T cell activation results in an autonomous program of cellular proliferation and differentiation. However, the mechanisms that underpin this process are unclear. Here, we profile genome-wide changes in chromatin accessibility, gene transcription, and the deposition of a key chromatin modification (H3K27me3) early after naive CD8$^+$ T cell activation. Rapid upregulation of the histone demethylase KDM6B prior to the first cell division is required for initiating H3K27me3 removal at genes essential for subsequent T cell differentiation and proliferation. Inhibition of KDM6B-dependent H3K27me3 demethylation limits the magnitude of an effective primary virus-specific CD8$^+$ T cell response and the formation of memory CD8$^+$ T cell populations. Accordingly, we define the early spatiotemporal events underpinning early lineage-specific chromatin reprogramming that are necessary for autonomous CD8$^+$ T cell proliferation and differentiation.

INTRODUCTION

Upon virus infection, naive, cytotoxic T lymphocyte (CTL) activation results in a largely autonomous program of differentiation that results in proliferation and acquisition of lineage-specific effector functions (van Stipdonk et al., 2003). The acquisition of lineage-specific CTL functions, such as the production of pro-inflammatory cytokines interferon gamma (IFN-γ) and tumor necrosis factor (TNF) (Denton et al., 2011; La Gruta et al., 2004) and expression of cytolytic effector molecules (Jenkins et al., 2007; Kägi et al., 1994; Moffat et al., 2009; Peixoto et al., 2007), helps limit and clear virus infection. Once the infection is cleared, the expanded effector CTL population contracts, leaving a pool of long-lived, pathogen-specific memory T cells. In contrast to naive CD8$^+$ T cells, virus-specific memory CTLs are able to respond more readily and rapidly to subsequent infections without the need for further differentiation (Kaech et al., 2002; La Gruta et al., 2004; Lalvani et al., 1997; Oehen and Brduscha-Riem, 1998; Veiga-Fernandes et al., 2000). This function enables rapid control of a secondary infection, leading to immune protection.

Optimal virus-specific CD8$^+$ T cell differentiation is underpinned by the coordinated expression of several transcription factors (TFs). The BATF TF has been shown to act early after activation and works in tandem with IRF4 and JUN family members to regulate transcriptional activation of gene loci involved in early immune T cell activation, cell survival, and metabolic pathways (Kurachi et al., 2014; Xin et al., 2016). Failure to engage BATF/JUN/IRF4-dependent programs results in diminished CD8$^+$ T cell expansion and function. BATF/JUN/IRF4 activity also results in subsequent upregulation of other TFs, such as T-BET (encoded by *Tbx21*), RUNX3, and BLIMP1 (encoded by *Prdm1*), which are all known to be essential for effective CD8$^+$ T cell differentiation (Cruz-Guilloty et al., 2009; Kallies et al., 2009; Kurachi et al., 2014; Wang et al., 2018; Xin et al., 2016). The activation of T-BET and RUNX3 consolidate commitment to the effector CTL lineage (Cruz-Guilloty et al., 2009; Intlekofer et al., 2005, 2008), whereas BLIMP1 is required for terminal

effector CTL differentiation (Kallies et al., 2009). These data demonstrate that the stepwise progression of TF expression during virus-specific CTL differentiation is critical for optimal responses. Interestingly, although as few as 2 h of antigenic stimulation is sufficient to initiate $CD8^+$ T cell proliferation (van Stipdonk et al., 2001), sustained stimulation for at least 20 h is required to install an optimal effector response (van Stipdonk et al., 2003). Although this information suggests that extensive cellular reprogramming prior to the first cell division is required to ensure optimal $CD8^+$ T cell responses, the exact molecular events that trigger this process are not fully understood.

We and others have demonstrated that virus-specific CTL differentiation is associated with genome-wide changes in chromatin accessibility and histone post-translational modifications (PTMs) (Denton et al., 2011; Northrop et al., 2008; Russ et al., 2014, 2017; Scott-Browne et al., 2016; Sen et al., 2016; Wang et al., 2018; Wei et al., 2009; Zediak et al., 2011). More recently, extensive changes in chromatin accessibility, indicative of transcriptional activation, was shown to occur prior to first cell division and was dependent on RUNX3 (Wang et al., 2018). Our own analysis showed that in the naive state, there is co-deposition of histone modifications associated with transcriptional activation (H3K4me3) and repression (H3K27me3) at $CD8^+$-T-cell-lineage-specific gene promoters and enhancers (Russ et al., 2014, 2017). Upon T cell activation, loss of H3K27me3 at gene promoters and enhancers was broadly associated with transcriptional upregulation of these poised genes (Russ et al., 2014). These data suggest that the presence of H3K4me3 at specific gene loci ensures that the genome of naive $CD8^+$ T cells is preconfigured for transcriptional activation, but it is maintained transcriptionally poised via co-localization of H3K27me3. Although removal of H3K27me3 appears to be a key step in the initiation of naive T cell activation, the timing, genomic targets, and specific molecular mechanisms of this initiating event remain to be determined.

The removal of H3K27me3 is specifically catalyzed by KDM6A and KDM6B demethylases (Agger et al., 2007). In mature $CD4^+$ T cells, KDM6A activity was required for the rapid expression of several key TFs, such as T-BET and STAT family members (LaMere et al., 2017). *Kdm6b*-deficient $CD4^+$ T cells demonstrate dysregulated and inappropriate fate specification under T helper (T_H) skewing conditions with promotion of T_H2/T_H17 lineages at the expense of T_H1 and FOXP3 T regulatory cells (Li et al., 2014). Together, these data suggest that dynamic modulation of H3K27me3 appears to be critical for multiple stages of T cell differentiation, both during development and activation. However, precisely how modulation of H3K27me3 during the very early stages of T cell activation promote effective T cell immunity is not fully understood.

There is little understanding of the respective roles of KDM6A and KDM6B in mediating H3K27me3 removal in and how this may facilitate CD8 T cell differentiation. Here, we determine that KDM6B is rapidly upregulated upon T cell activation and prior to first cell division. This coincides with a stepwise engagement of transcriptional modules that were linked with rapid H3K27me3 demethylation. This occurred at genes involved in a broad range of cellular support processes that underpin optimal T cell activation and proliferation. Initial H3K27me3 demethylation and increased chromatin accessibility targeted regions enriched for BATF/IRF/JUN binding sites, with T-BET and GATA TF binding sites (TFBS) evident at later stages of H3K27me3 demethylation. Small molecule and short hairpin RNA (shRNA) inhibition of KDM6B-dependent H3K27me3 demethylation limited the magnitude of an effective primary virus-specific $CD8^+$ T cell response and formation of functional memory $CD8^+$ T cell populations capable of recall. Our data show that H3K27me3 methylation acts as a molecular handbrake on the initiation of effective T cell responses, with H3K27me3 demethylation being a key step at the very earliest stages of T cell activation, enabling optimal lineage-specific reprogramming of effector and memory $CD8^+$ T cells.

RESULTS

Rapid upregulation of *Kdm6b* occurs after naive $CD8^+$ T cell activation

To better understand the global transcriptional changes associated with the rapid loss of H3K27me3, naive ($CD44^{int/lo}CD62L^{hi}$) OT-I $CD8^+$ T cells were sorted after *in vitro* activation with their cognate peptide antigen, the ovalbumin ($OVA_{257-264}$, SIINFEKL) N4 peptide. Changes in gene transcription at early (3 and 5 h) and late (24 h) times post-stimulation were assessed by RNA sequencing (RNA-seq). We initially assessed the transcriptional dynamics of chromatin modifiers at early (3–5 h) and late (24 h) time points after activation (Figure 1A; Table S1). Interestingly, we observed upregulation across the time course of histone methyltransferases, such as *Suv39h1/h2* and *Ezh2/Suz12*, that are associated with deposition of H3K9me3 (Rea et al., 2000) and H3K27me3 (Cao et al., 2002), respectively. This result is in line with recent reports showing that upregulation of these components are important for optimal effector $CD8^+$ T cell responses (Gray et al., 2017; Pace et al., 2018). We also observed that the H3K27me3 demethylase *Kdm6b* was transiently upregulated at 3 and 5 h but returned to levels observed in naive OT-I $CD8^+$ T cell levels at 24 h (Figure 1A). This trend was also observed in anti-CD3-stimulated naive $CD8^+$ T cells isolated from C57BL/6 mice (Figure S1A), irrespective of the presence of interleukin-2 (IL-2). *Kdm6b* was the only one of five histone demethylases analyzed that was transcriptionally upregulated in response to TCR activation, whereas *Kdm6a*, another histone demethylase that is responsible for H3K27me3 removal, remained unchanged (Figure 1B). *In vitro* stimulation with different N4 peptide variants demonstrated that *Kdm6b* upregulation was only responsive to higher TCR affinity peptides, namely, N4 and Q4, compared to the lower affinity E1 and G4 variants (Figure S1B). These results clearly demonstrate *Kdm6b* upregulation reflects the quality of TCR-driven activation within these naive OT-I $CD8^+$ T cells.

Rapid H3K27me3 demethylation occurs after naive $CD8^+$ T cell activation

TCR-signaling-induced *Kdm6b* upregulation coincided with a progressive loss of H3K27me3 at the promoters of the key TFs *Irf4*, *Tbx21*, and *Irf8* at 5 and 24 h after activation, whereas the levels of H3K4me3 enrichment remained consistent across these time points (Figure 1C). This progressive loss of

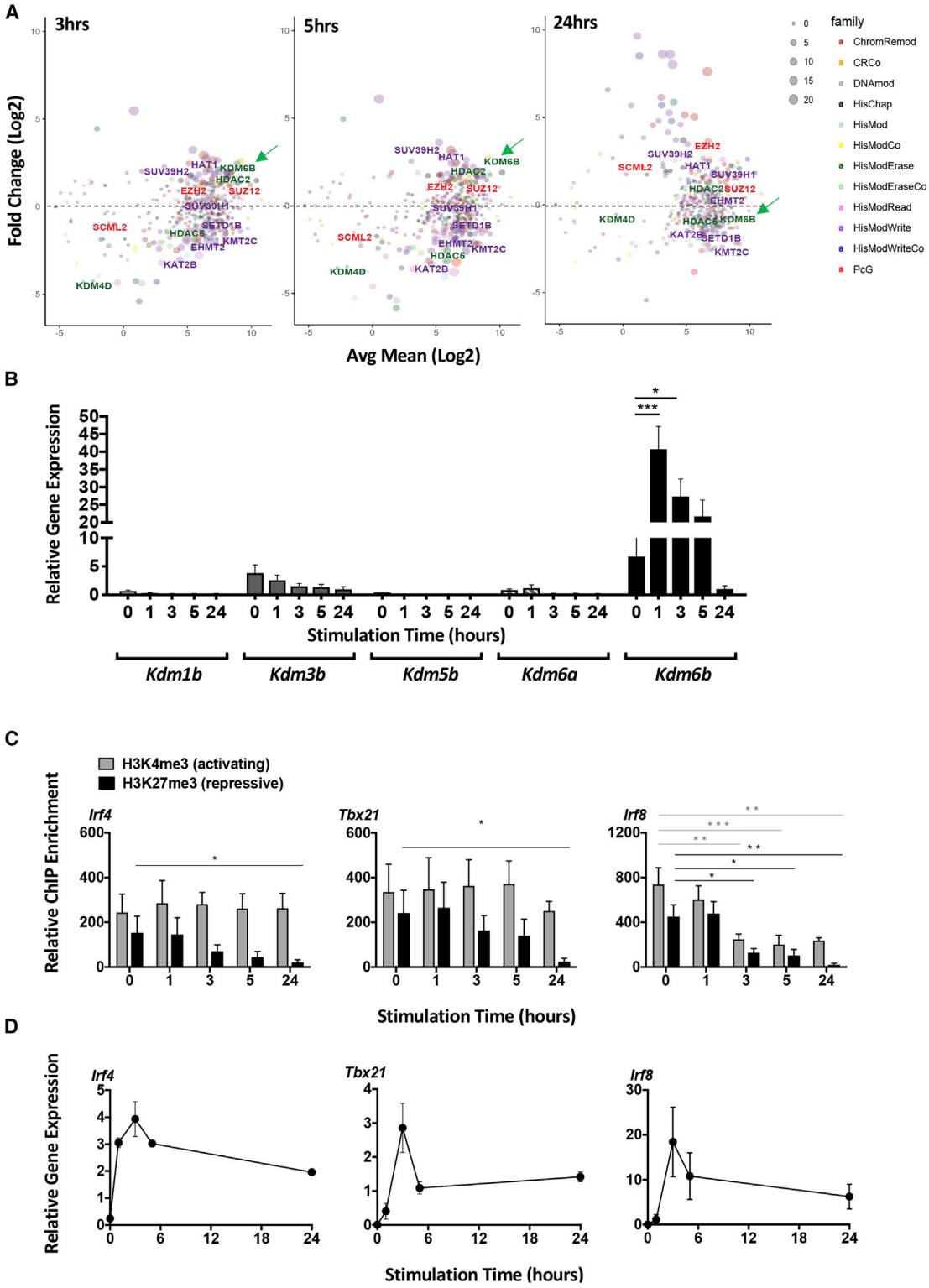

Figure 1. The regulation of *Kdm6b* and H3K27me3 demethylation during early hours of T cell activation

(A) RNA-seq analyses were performed on naive ($CD44^{lo}CD62L^{hi}$) $CD45.1^{+}$ $CD8^{+}$ OT-I T cells that were either left unstimulated or stimulated with the N4 peptide in the presence of rhIL-2 (10 U/mL) for 3, 5, and 24 h. The expression fold change (log_2) of histone modifiers in these activation time points was compared to unstimulated OT-I naive $CD8^{+}$ T cells.

(B) Relative gene transcription levels of *Kdm1b*, *Kdm3b*, *Kdm5b*, *Kdm6a*, and *Kdm6b* were validated by qPCR.

(legend continued on next page)

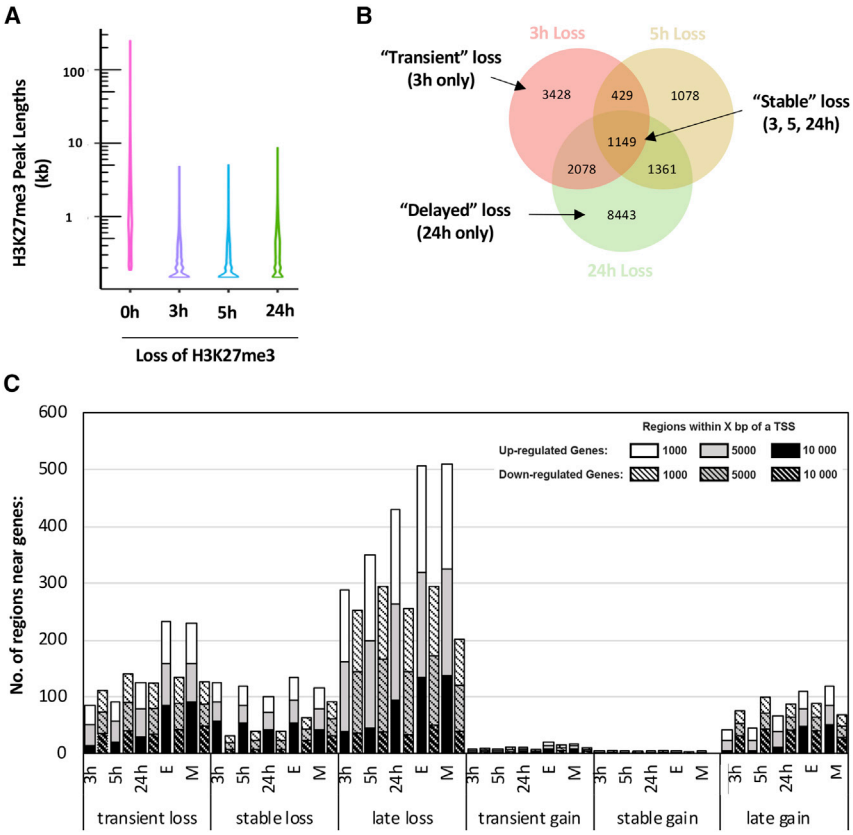

Figure 2. Dynamic regulation of H3K27me3 during early CD8$^+$ T cell activation

(A) H3K27me3 ChIP-seq was performed on either naive CD8$^+$ OT-I T cells or on OT-I T cells after 3, 5, or 24 h of *in vitro* stimulation as described above in Figure 1. Data were mapped back to the mouse genome (version mm10). H3K27me3 domain length was assessed within regions that exhibited a loss of H3K27me3 within activated CD8$^+$ T cells compared to naive CD8$^+$ T cells.

(B) Genomic regions that marked with H3K27me3 within OT-I CD8$^+$ T cells activated for 3, 5, and 24 h were enumerated and compared to H3K27me3 regions within unstimulated naive OT-I T cells. Genomic regions exhibiting H3K27me3 loss only after 3 h of stimulation were characterized as "transient" loss; decreased H3K27me3 at 3, 5, and 24 h of stimulation were "stable" loss; and decreased H3K27me3 at 24 h only after stimulation as "delayed" loss.

(C) H3K27me3 ChIP-seq was performed on either naive CD8$^+$ OT-I T cells or on OT-I T cells simulated as described above in Figure 1. Data were mapped back to the mouse genome (version mm10). Genomic regions that either lost or gained H3K27me3 within activated CD8$^+$ OT-I T cells were compared to the unstimulated sample. These regions were categorized into either transient, delayed, or stable loss or gain of H3K27me3. The number of regions in the groups of transient, stable, or delayed H3K27me3 loss and gain were within 1,000, 5,000, or 10,000 base pairs (bp) of the transcription start site of differentially expressed genes identified after *in vitro* activation (see Figure 1) or identified after a 50-h stimulation of *ex-vivo*-derived effector OT-I CD8$^+$ T cells (Russ et al., 2014).

H3K27me3 appeared to be selective, as H3K27me3 remained largely constant at the promoter of *MyoD* and *Actin* (Figure S1C). Furthermore, the removal of H3K27me3 coincided with concomitant transcriptional upregulation of these TFs (Figure 1D).

To identify the genomic regions that underwent rapid H3K27me3 demethylation, we carried out H2K27me3 chromatin immunoprecipitation sequencing (ChIP-seq) at 3, 5, and 24 h after naive T cell activation (Figure 2). Consistent with previous reports (Araki et al., 2009; Russ et al., 2014), naive CD8$^+$ T cells exhibited broad H3K27me3 regions (Figure 2A). Upon CD8$^+$ T cell activation, H3K27me3 domains were trimmed significantly, with this remodeling maintained up to 24 h (Figure 2A). H3K27me3 demethylation was evident at 7,137, 4,022, and 13,077 regions at 3, 5, and 24 h, respectively (Figure 2B), far exceeding the number of regions that had gained H3K27me3 (518, 3,641, and 2,342 regions, at 3, 5, and 24 h, respectively) (Figure S2A). Both a gain and loss in H3K27me3 levels occurred directly at the promoter, the transcription start site (TSS), exons, 5′ UTR, and 3′ UTR of a gene, with most H3K27me3 changes annotated to introns, intergenic regions, and short interspersed elements (SINEs) (Figure S2B), indicating the role of H3K27me3 in regulating both protein-coding and non-coding regions.

To investigate the dynamics of H3K27me3 demethylation, we classified regions based on the timing of H3K27me3 removal. We observed that 3,428 regions (48%) were transiently demethylated, exhibiting a decrease in H3K27me3 at 3 h (transient loss). In contrast, relatively few regions (1,149, 16.1%) were stably demethylated at all time points measured (3, 5, and 24 h; stable loss). Of the 13,077 regions demethylated at 24 h, the majority of them (8,443, 65%) only showed demethylation at the 24-h time point (delayed loss) (Figure 2B). These data are indicative of a staged H3K27me3 demethylation within the first 24 h of naive T cell activation. Given that the numbers of regions exhibiting a "transient," "stable," and "delayed" gain in H3K27me3 were significantly smaller than those that lost H3K27me3 (Figure S2B), we primarily focused on regions that exhibited H3K27me3 demethylation early after T cell activation.

(C) Relative enrichment of H3K27me3 measured by ChIP-qPCR by using primers spanning across the promoter of *Irf4*, *Tbx21*, and *Irf8* gene loci in OT-I CD8$^+$ T cells stimulated up to 2 h in 10 U/mL of rhIL-2 with the 1-μg N4 peptide *in vitro*.

(D) Relative gene transcription measured by quantitative real-time PCR validated the transcriptional pattern of the transcription factors *Tbx21* (encodes T-BET), *Irf4* (IRF4), and *Irf8* (IRF8) in OT-I naive CD8$^+$ T cells stimulated as described above. Data are shown as mean ± SEM from 3 independent repeats with statistical significance calculated using a one-tailed Student's t test (*$p < 0.05$ **$p < 0.01$, ***$p < 0.001$).

Early H3K27me3 demethylation initiates cellular processes required during effector and memory differentiation

To understand how early H3K27me3 demethylation impacted the gene expression profiles observed in early activated CD8$^+$ T cells, H3K27me3 demethylated regions were annotated to nearest neighboring differentially expressed genes (DEGs; ±10 kb). Within early hours of T cell activation, the majority of the regions exhibiting stable and delayed demethylation were associated with transcriptionally active genes, rather than downregulated genes (Figure 2C). Importantly, this association continued to be evident in *ex-vivo*-derived effector and memory CD8$^+$ OT-Is (Figure 2C), indicating that these early changes in H3K27me3 demethylation are associated with transcriptional upregulation and are transmitted into effector and memory CD8$^+$ T cells.

To visualize H3K27me3 dynamics, we generated heatmaps showing the tag density within H3K27me3 peaks (±5 kb from the center of the peak) annotated to the nearest neighboring gene (Figure 3A). Interestingly, regions that exhibited rapid demethylation that were stable at the 24-h time point were linked to genes with a well-documented role in T cell biology and cell cycle processes (Figure 3A). Interestingly, there appears to be a great overlap between genes annotated to lists of stable, transient, and delayed regions. These H3K27me3 demethylated regions could potentially be putative enhancers belonging to the same gene that undergo different patterns of demethylation during early T cell activation.

Gene Ontology analysis demonstrated that regions exhibiting transient demethylation were primarily involved in chemokine and cellular migration processes. Interestingly, gene loci that exhibited stable and/or delayed demethylation were enriched for general cellular processes, such as cytokine production, cell growth, cell morphogenesis, cell adhesion, proliferation, and cell cycle arrest (Figure 3B). To further understand the role of H3K27me3 removal in T cell commitment, we identified H3K27me3 demethylated regions that overlapped with those in effector/memory CD8$^+$ T cells and those that do not overlap (Figure S2C), followed by gene annotation and pathway analysis (Figure S2D). Corroborating with our previous result, genomic regions with stable or delayed H3K27me3 removal during early T cell activation indeed overlapped with demethylated regions in fully differentiated effector and memory CD8$^+$ T cells. They were annotated to genes enriched in pathways such as response to cytokines, activation of immune responses, and regulation of lymphocyte proliferation. With the exception to cellular response to cyclic 3′,5′-guanosine monophosphate and signal transduction in gene regulation, we could not identify any memory-associated pathways that specifically arise after the first cell division. Instead, we identified an enrichment of pathways such as phosphatidylinositol 3-kinase (PI3K)-Akt, mitogen-activated protein kinase (MAPK), and Wnt signaling not only in fully differentiated effector and memory but also in group of genes that experience delayed demethylation within the first 24 h of T cell activation. These results therefore strongly indicate that early H3K27me3 removal within hours of T cell activation is critical for initiating proliferative, inflammatory, and lineage-commitment pathways necessary for effector and memory T cell differentiation.

To explore this further, we carried out Gene Ontology of DEGs identified at 3, 5, and 24 h after activation in our RNA-seq data. K-means clustering partitioned DEGs into modules of transcriptionally induced (sets a–d) or repressed genes (sets e–h) that exhibited distinct kinetics (Figures S3A and S3B). Gene Ontology analysis of DEGs that were upregulated after activation showed distinct functional associations depending on when they were upregulated. Genes that were rapidly but transiently upregulated (set a) were enriched in genes associated with inflammatory and immune response function (Figure S3C). Genes that were transcribed over the entire time course (sets b and c; 3–24 h) were enriched for cellular support processes, such as RNA binding and processing, metabolic pathways, and cell cycle/proliferation processes (Figure S3C). Finally, those genes upregulated at 24 h only were enriched for DNA repair and cellular division (Figure S3C). Taken together, our data demonstrate that naive CD8$^+$ T cell activation results in rapid H3K27me3 demethylation resulting in stepwise engagement of transcriptional modules important for readying the activated T cell for subsequent proliferation and differentiation.

H3K27me3 removal establishes a permissive chromatin landscape for TF binding

Naive T cell activation was associated with a loss of histone H3 and concomitant increase in chromatin accessibility at the *Irf4*, *Tbx21*, and *Irf8* promoters (Figure 4A). To assess the link between increased chromatin accessibility and H3K27me3 demethylation at a genome-wide scale, we performed assay for transposase-accessible chromatin using sequencing (ATAC-seq) at early and late activation time points (0, 3, and 24 h) and cross referenced it to the H3K27me3 ChIP-seq data at the same time points. A significantly greater number of regions (27.5%) that exhibited stable H3K27me3 loss at 3 h also exhibited an increase in chromatin accessibility compared to regions with transient or delayed H3K27me3 demethylation (10%) (Figure 4B). Importantly, regions that exhibited concomitant H3K27me3 loss and increased chromatin accessibility were associated with transcriptionally upregulated genes at the same time points (Figure S4).

To determine if H3K27me3 demethylation patterns (transient, stable, and delayed) detected during the first 24 h of T cell activation were maintained in fully differentiated virus-specific T cells isolated directly *ex vivo*, early demethylation datasets were cross referenced against H3K27me3 methylation datasets obtained from *ex-vivo*-derived effector and memory T cells (Russ et al., 2014). Many of the genomic regions exhibiting demethylation initiated within the first 24 h of T cell activation remained demethylated in fully differentiated effector (E) and memory (M) T cells (Figure S4). Concomitantly, these same demethylated regions also showed increased H3K27ac deposition in effector and memory compared to naive T cells (Figure S4). This analysis therefore indicates a number of these genomic regions exhibiting chromatin remodelling prior to first cell division were also observed in mature *ex vivo* effector and memory influenza A virus (IAV)-specific CTLs. Together, these findings suggest that early H3K27me3 demethylation is an integral step that results in a rapid transition to a permissive chromatin landscape early after naive T cell activation and that is maintained in mature virus-specific effector and memory CTLs.

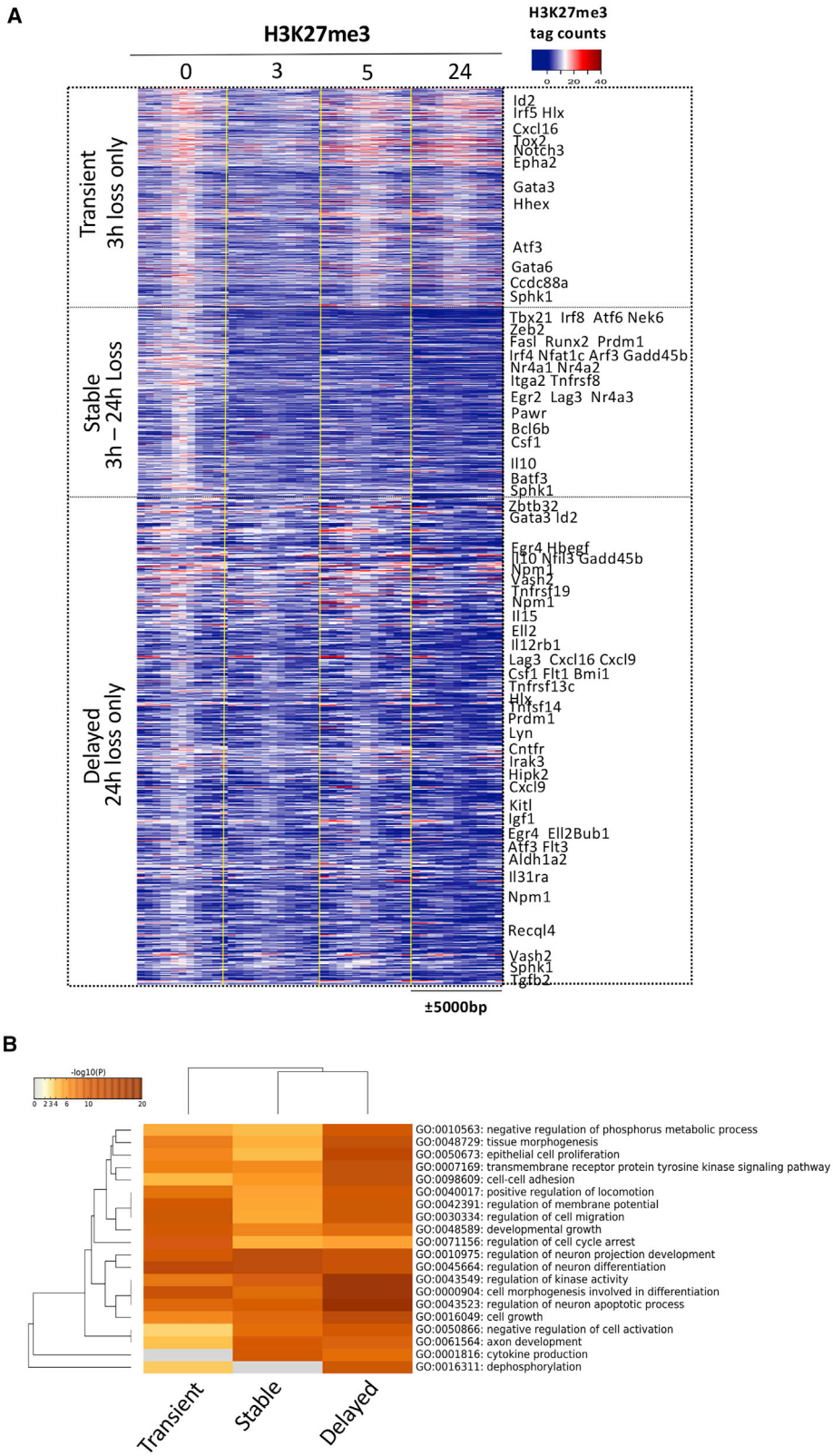

(legend on next page)

Given the link between the loss of H3K27me3 and increased chromatin accessibility, we next assessed which TF binding motifs were enriched at H3K27me3 demethylated regions at 3, 5, and 24 h after activation (Figure 4C). Interestingly, in line with the stepwise induction of specific transcriptional modules at distinct stages of early T cell activation (Figure S3), we observed staged enrichment for specific TF motifs at 3, 5, and 24h after T cell activation. ATF/JUN motifs were among one of the earliest motifs detected at demethylated regions at 3 h post-activation (Figure 4C; Figure S5A) and increasing up to 24 h. At 5 h after activation, TF motifs for REL, IRF/STAT/GATA family members emerged at H3K27 demethylated regions with the later appearance of TBX21, RUNX3, and NFIL3 motifs at demethylated regions at 24 h. Interestingly, motifs for EGR and E2F TFs were only transiently enriched (3 h) and were negatively enriched at regions demethylated at 5 and 24 h after T cell activation. Hence, dynamic regulation of H3K27 methylation upon naive T cell activation results in ordered chromatin remodeling events that appear to ready the chromatin landscape for specific TF binding.

To determine whether enrichment of TF motifs at H3K27me3 demethylated sites corresponded to specific TF binding, regions that exhibited loss or gain of H3K27me3 were overlaid with publicly available T cell TF ChIP-seq data (Figures 4D and 4E). Supporting the TF motif enrichment analysis (Figure 4C), stably demethylated regions in recently activated $CD8^+$ T cells were enriched for AP-1 (JUND, 14.6%; BATF, 15.2%; FOSL, 2%–11.6%) and STAT (STAT, 1%–13.3%; STAT, 3%–10.2%; STAT5A, 11.8%) members and TBX21 (12.1%) and IRF4 (15.4%) binding compared to either the transiently or delayed groups, which ranged between 2% and 6% in the same dataset (Figures 4D and 4E). In contrast, 19.3% of the transiently H3K27 demethylated regions and 17%–20% of the regions exhibiting H3K27me3 gain overlapped with SUZ12 binding, a component of the PRC2 complex that is responsible for H3K27me3 deposition (Figures 4D and 4E). This finding suggests that the observed upregulation of PRC2 components, namely, EZH2 and SUZ12, early after T cell activation may correlate with remethylation of transiently demethylated regions soon after T cell activation (Gray et al., 2017).

Importantly, a greater percentage of stably demethylated regions (21.8%) also showed binding for the histone acetyltransferase p300 compared to the transient demethylated regions (8.8%; Figures 4D and 4E). The potential for p300 binding at these stably demethylated regions was linked to genes that were transcriptionally induced in effector and/or memory T cells (Figure S4). These data suggest that p300 binding and subsequent acetylation of H3K27 are required for the demethylation to remain stable instead of transient. To test this hypothesis, we overlaid our previous H3K27ac data from naive, effector, and memory $CD8^+$ T cells (Russ et al., 2017) with transiently, stable, and delayed H3K27me3 demethylated regions. In comparison to the transiently demethylated regions, there was a greater proportion of the stably demethylated regions that either overlapped (10%) or were within 2 kb (25%) or 5 kb (38%) of a region with increased H3K27ac in effector T cells (Figure 5). This trend was similarly observed in memory T cells, albeit at lower percentages (Figure 5). These overlapping regions with stable demethylation in early hours of T cell activation and effector and memory T cells were positioned near DEGs linked to $H3K27Ac^+$ regions (Figure S5B). Together, these data support the notion that early H3K27me3 demethylation enables increased chromatin accessibility, and this is further stabilized by the binding of p300 and subsequent H3K27 acetylation.

Inhibition of H3K27 demethylations limits $CD8^+$ effector T cell differentiation

Naive OT-I $CD8^+$ T cells treated with GSK-J4, a small-molecule inhibitor, which binds to the catalytic pocket of KDM6B (Kruidenier et al., 2012), were activated with the N4 peptide for 0, 1, 3, 5, and 24 h (Figure 6A). GSK-J4 inhibition of KDM6B activity prevented the removal of H3K27me3 and transcriptional upregulation of *Tbx21*, *Irf4*, and *Irf8*, without affecting pre-existing H3K4me3 levels when compared to both mock-treated and OT-I T cells treated with a non-functional analog (GSK-J5) (Figures 6A and 6B).

To determine whether GSK-J4 treatment of naive OT-I $CD8^+$ T cells would impact virus-specific $CD8^+$ T cell differentiation, naive OT-I T cells were treated with the GSK-J4 inhibitor or GSK-J5 analog for 4 h *in vitro*. An equal number of OT-I T cells were then adoptively transferred into recipient B6 mice infected 3 days prior to transfer with the A/HKx31-OVA virus (Jenkins et al., 2006; Figure 6C). At 3 days after transfer, both the proportion and absolute number of GSK-J4-treated OT-I $CD8^+$ T cells were reduced compared to those of the the mock- or GSK-J5-treated OT-I $CD8^+$ T cells (Figure 6C). Although both mock- and J5-treated OT-I T cells had undergone extensive cell division (Figures 6D–6F), GSK-J4-treated OT-I $CD8^+$ T cells had undergone fewer divisions (Figure 6F). Therefore, the inability to efficiently demethylate H3K27me3 early after $CD8^+$ T cell activation resulted in a diminished capacity to fully engage the proliferative capability of virus-specific $CD8^+$ T cells in response to infection.

Examination of functional characteristics of the responding OT-I T cells demonstrated that early H3K27 methylation was also required for upregulation of key TFs (T-BET and GATA3) (Figures S6A and S6B), and interestingly, there was a lower proportion of GSK-J4-treated OT-I T cells located within the draining lymph node producing IL-2, IFN-γ, or TNF upon reactivation than mock-treated and GSK-J5-treated cells (Figures S6C–S6E). This was also reflected in a diminished proportion of multifunctional OT-I T cells isolated from the draining lymph node capable of simultaneously producing all three cytokines (Figures S6F and S6G). Hence, H3K27 demethylation, prior to initial cell division,

Figure 3. H3K27me3 demethylation regulates genes involved in cellular support processes

(A) The total number of H3K27me3 sequence tags within ±5 kb of the middle of the peak was transformed (log2) and converted into a heatmap according to Russ et al. (2014). Hierarchical clustering was then used to identify genomic regions that exhibited similar patterns of transient, stable, or delayed H3K27me3 loss. These regions were then annotated to thenearest neighbor genes (listed).

(B) Gene Ontology (GO) analysis of annotated gene loci linked to H3K27me3 regions exhibiting transient, stable, or delayed loss of H3K27me3 was carried out, and hierarchical clustering based on p value was carried out.

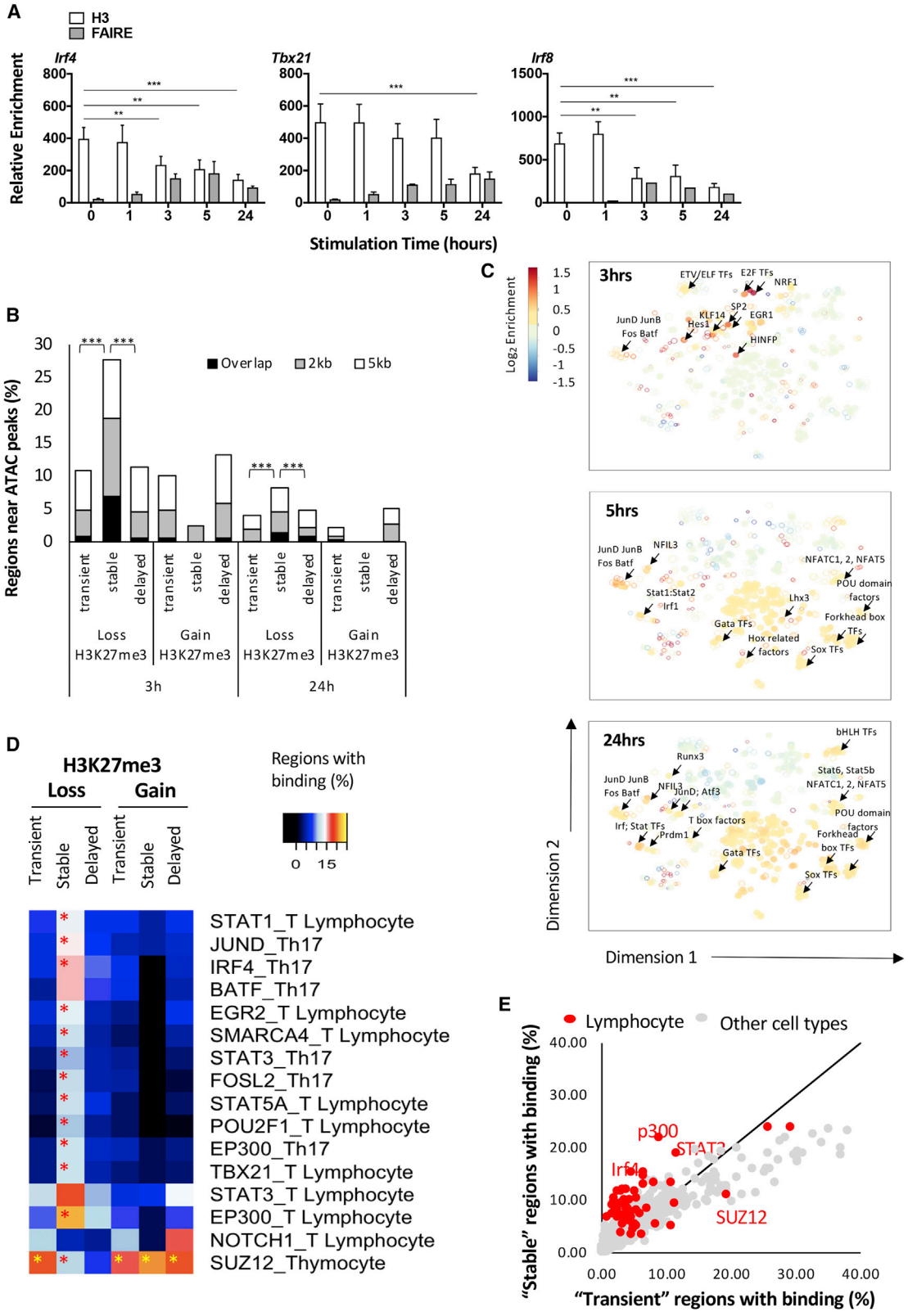

(legend on next page)

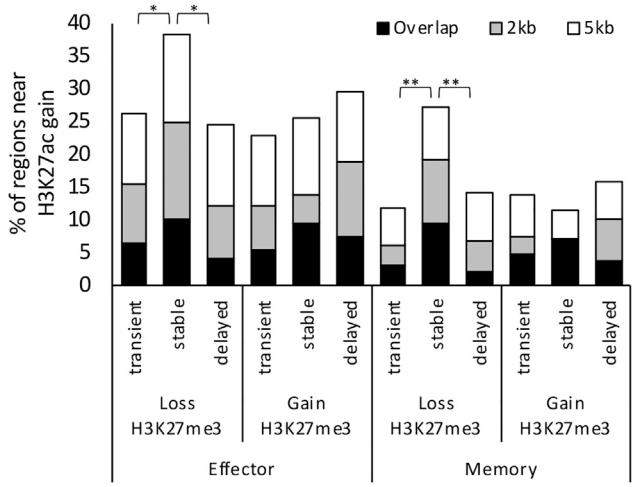

Figure 5. Genomic regions that exhibit H3K27me3 loss are associated with gain of H3K27Ac

The proportion (%) of genomic regions identified to exhibit H3K27me3 demethylation that also overlapped (within 0 to 5 kb) to a region that exhibited H3K27Ac gain within effector or memory OT-I CD8$^+$ T cells (Russ et al., 2014) is shown. A significantly higher proportion of regions with stable demethylation overlapped or were within <5 kb to a H3K27Ac-enriched region in effector (*p < 2.2e−16) and memory (**p < 6.5e−5) OT-I CD8$^+$ T cells than those with transient or delayed demethylation.

appears to be a critical step for initiation of the autonomous CD8$^+$ T cell differentiation program induced by T cell activation.

H3K27me3 removal is required for establishing virus-specific CD8$^+$ T cell memory

We next determined whether CD8$^+$ T cell memory T cell formation was left intact after inhibition of KDM6B-dependent H3K27me3 demethylation prior to initial activation. The primary and secondary responses of adoptively transferred OT-I T cells treated with either the GSK-J5 analog or the GSK-J4 drug were then assessed after primary challenge (A/HKx31-OVA; day 10), memory (day 30), or after secondary challenge (A/PR8-OVA; day 6) (Figure 7A). In support of our earlier data, GSK-J4 treatment had a profound impact on the expansion of OT-I CD8$^+$ T cells optimal during the primary acute effector response. The diminished primary response observed after GSK-J4 treatment of OT-I CD8$^+$ T cells was also reflected in the establishment of a lower memory OT-I cell frequency in the spleen (Figure 7B). A comparison of OT-I CD8$^+$ T cell numbers in the lung tissue 30 days after primary infection demonstrated that GSK-J4 treatment prior to adoptive transfer resulted in a significantly reduced frequency and number of total memory OT-I CD8$^+$ T cells (Figure 7C). Utilizing intravital injection of anti-CD3 antibody to distinguish resident versus circulating memory CTL, we determined that GSK-J4 treatment also resulted in fewer tissue-resident CD69$^+$CD103$^+$ memory OT-Is (Figure 7D). Thus, it appears that inhibition of H3K27me3 demethylation impacted the formation of effector and memory CTL populations.

To determine whether inhibiting H3K27me3 demethylation also impacted the recall capacity of established memory OT-I, we secondarily challenged primarily infected mice that had received GSK-J4-, J5-, or mock-treated OT-Is with a serologically distinct A/PR8 strain of IAV-OVA (Figures 7B and 7E). Memory OT-I T cells established after transfer and primary activation of GSK-J4-treated OT-Is failed to expand upon secondary infection. This was evident in the spleen (Figure 7B), the bronchoalveolar lavage fluid (BAL), and mediastinal lymph node (mLN) (Figure 7E). Together, these data suggest that a failure to remove H3K27me3 early after activation impacts not only initial T cell expansion but also programming of memory recall potential. This was likely not due to a difference in starting memory T cell number, as the fold expansion in GSK-J4-treated mice was significantly diminished compared to that of the GSK-J5 controls. This finding indicates an intrinsic defect in recall capacity.

To further consolidate our finding that KDM6B plays a role in programming optimal CD8$^+$ T cell memory, we used transgenic mice that constitutively express a *Kdm6b*-specific shRNA, for constitutive knockdown of *Kdm6b* (Prier et al., 2019a). The mice express *Kdm6b* mRNA as part of a GFP reporter for which the levels of GFP are indicative of shRNA levels (Prier et al., 2019a). Expression of the *Kdm6b* shRNA knocked down *Kdm6b* transcription by ~50% in naive CD8$^+$ T cells compared to the luciferase shRNA control (Figure S6H). We observed that

Figure 4. Stable H3K27me3 removal at genomic regions targeted by T-cell-specific TFs

(A) Naive OT-I CD8$^+$ T cells were activated as previously described above. Changes in chromatin accessibility was assessed by FAIRE-qPCR and H3 histone ChIP using qPCR and primers specific the *Irf4*, *Tbx21*, and *Irf8* promoters. Data are shown as mean ± SEM from 3 independent repeats with statistical significance calculated using a one-tailed Student's t test (*p < 0.05 **p < 0.01, ***p < 0.001).

(B) Genome-wide changes in chromatin accessibility was assessed by ATAC-seq on naive OT-I CD8$^+$ T cells or activated for 3 and 24 h. Shown is the proportion (%) of regions exhibiting distinct H3K27me3 demethylation dynamics that either directly overlapped or were positioned within 2 to 5 kb to the center of called ATAC-seq peaks. A significantly higher percentage of regions with stable demethylation overlapped or were within <5kb of a chromatin accessible region at 3 h and 24 h than those with transient or delayed demethylation (***p < 2.2e-16).

(C) Prediction of transcription factor binding sites within H3K27me3 demethylated regions was carried out using the CiiiDER algorithm (Gearing et al., 2019; Russ et al., 2017). Shown is a t-distributed stochastic neighbor embedding (t-SNE) plot displaying transcription factor motif enrichment (log_2) within H3K27me3 demethylated regions at 3, 5, and 24 h after T cell activation compared to H3K27me3 methylated regions common to all time points (0, 3, 5, and 24 h). Red circles represent highly enriched TFBS; blue circles represent TFBS that are under-represented. Open circles represent significantly enriched TF motifs that are present in at least 15% of gene loci.

(D) Publicly available TF ChIP-seq data for TFs identified to have significantly enriched TFBS (Figure 4C) were downloaded from GEO datasets. The data were mapped to regions exhibiting transient, stable, or delayed H3K27me3 demethylation, and the percentage (%) of regions exhibiting overlap of TF binding with either H3K27me3 demethylation or H3K27me3 gain was determined. *, indicates significantly greater binding percentages than all H3K27me3-enriched regions at 0 h (p < 0.01).

(E) The percentage of genomic regions exhibiting overlap in transcription factor binding in either stable or transient H3K27me3 demethylation were compared. Highlighted in red are publicly available TF ChIP-seq data derived from T cell populations, and TF binding data from other cell types are represented in gray. Gene loci exhibiting significant binding to stable regions or transient regions are named.

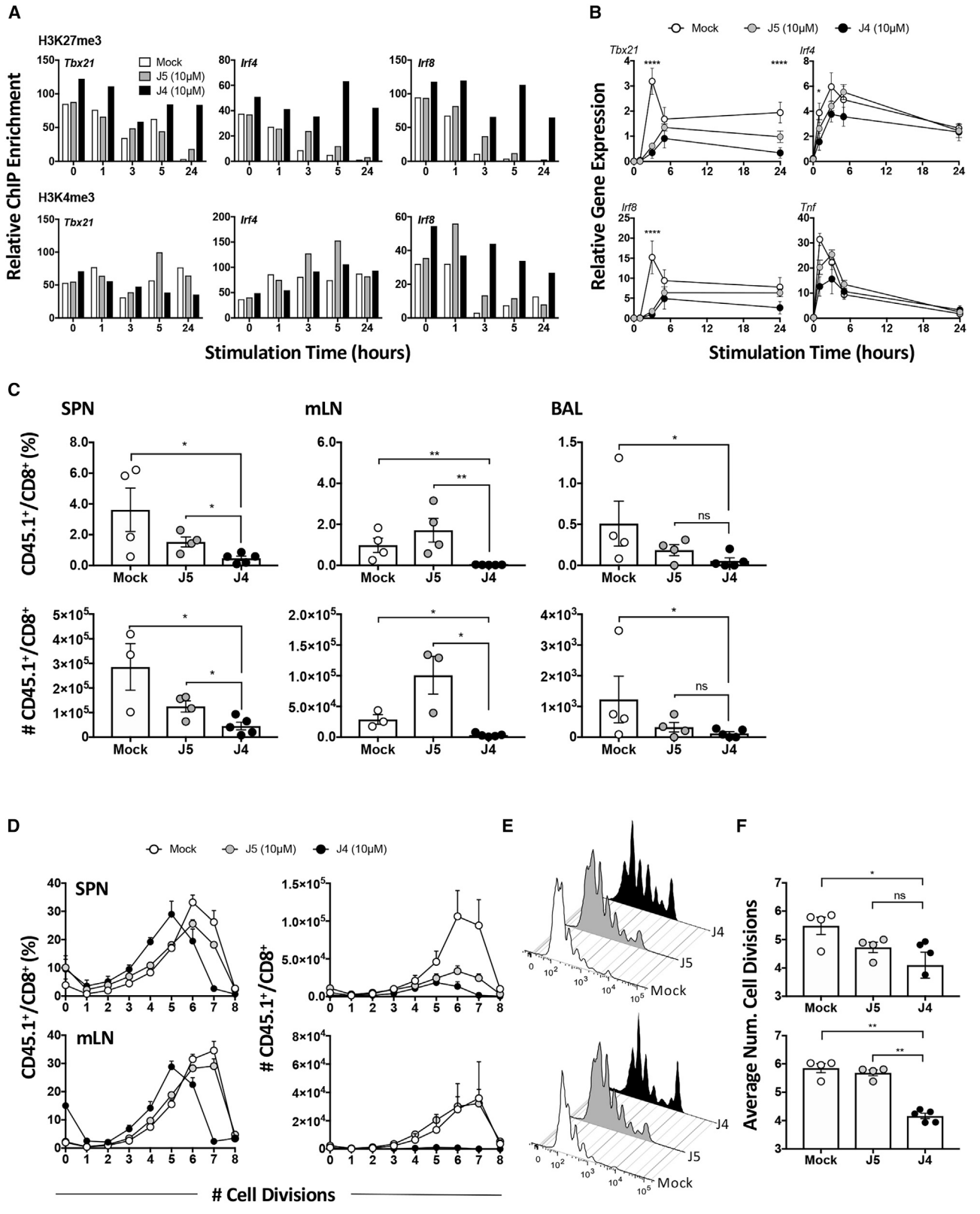

(legend on next page)

gene that exhibited transcriptional knockdown (at least 30%) significantly overlapped with gene loci/regulatory elements that exhibited H3K27me3 demethylation within the first 24 h after T cell activation (Figure 7F). These data provide further evidence that KDM6B-dependent H3K27 demethylation is a key step in transcriptional activation of target gene loci early after activation.

Kdm6b shRNA mice were infected with A/HKx31 and memory D^bNP_{366} and D^bPA_{224}-specific $CD8^+$ T cell responses analyzed in the spleen 30 days after infection. *Kdm6b* knockdown in GFP^{hi} $CD8^+$ T cells resulted in a diminished number of IAV-specific memory $CD8^+$ T cells compared to the luciferase shRNA knockdown controls (Figure 7G). This diminished response was reflected in lower proportion of both effector (T_{EM}) and central (T_{CM}) memory subsets. Altogether, both of these experimental models demonstrate that inhibition of KDM6B, and subsequent H3K27me3 demethylation during early T cell activation, is critical for facilitating not only mature primary virus-specific $CD8^+$ T cell expansion but also formation of functional virus-specific memory $CD8^+$ T cells.

DISCUSSION

Our study provides molecular evidence that initial T cell activation results in rapid KDM6B-dependent removal of H3K27me3, enabling engagement of transcriptional pathways required for preparing T cells for subsequent proliferation and differentiation. KDM6B-dependent removal of H3K27me3 enables increased chromatin accessibility and the staged exposure of specific TFBSs within gene regulatory elements. This is associated with subsequent histone acetylation and stable transmission of transcriptionally permissive chromatin structures into effector and memory CTL populations. Hence, within the first 24 h and prior to first cell division, remodeling of the chromatin landscape provides a platform enabling binding of T-cell-specific TFs. This information provides a molecular basis for engagement of the $CD8^+$ T cell proliferation and differentiation program induced by T cell activation. Inhibiting appropriate chromatin remodeling early after T cell activation negatively impacts subsequent optimal differentiation of virus-specific CTL and establishment of virus-specific $CD8^+$ T cell memory.

In this study, we demonstrated that TCR engagement specifically upregulated *Kdm6b* transcription, and not *Kdm6a,* which is another H3K27me3 demethylase. This differential H3K27me3 demethylase upregulation after TCR activation potentially explains the observation that virus-specific effector and memory $CD8^+$ T cell generation is normal in *Kdm6a* knockout mice (Cook et al., 2015; Yamada et al., 2019). Interestingly, T-cell-specific *Kdm6a* deficiency did restrict lymphocytic choriomeningitis virus (LCMV)-specific T follicular $CD4^+$ T cell responses, leading to increased susceptibility (Cook et al., 2015). This may point to distinct roles for KDM6A and KDM6B in $CD4^+$ and $CD8^+$ T cell responses, respectively.

Concurrent with KDM6B upregulation, we saw upregulation of the PRC2 H3K27me3 methyltransferase subunits *Ezh2* and *Suz12.* This finding raises an interesting question about how recently activated $CD8^+$ T cells initiate appropriate gene transcription when there is active competition between enzymes that write or erase H3K27me3. Our comprehensive profiling of H3K27me3 deposition in early-activated and *ex-vivo*-differentiated effector and memory T cells showed that regions that exhibited either delayed or stably maintained H3K27me3 demethylation were associated with an initial permissive chromatin state that was consolidated by $H3K27Ac^+$ enrichment and chromatin accessibility. Importantly, these regions exhibited significant overlap with publicly available ChIP-seq data identifying regions in activated T cells bound by the histone acetyltransferase P300. In contrast, regions that showed transient H3K27me3 demethylation overlapped with regions that were targets for the PRC2 subunit SUZ12. It is tempting to speculate that a rapid transition from methylation to acetylation at H3K27 acts as a molecular switch that ensures activation of stable gene transcription required for optimal T cell differentiation and proliferation. This then protects activated gene loci from the activity of opposing chromatin modifiers, ensuring stability of the differentiation state.

An analysis of genomic regions that lost H3K27me3 and became more accessible over the time course demonstrated staged exposure of specific TFBS before initial cell division. BATF/JUN binding sites emerged first, followed by STAT/IRF/NFAT/nuclear factor κB (NF-κB) sites and finally TBX/RUNX sites at 24 h after activation. The initial unmasking of regions containing BATF/JUN family binding sites fits with earlier observations that BATF acts as an important factor for the initiation of $CD8^+$ T cell activation (Godec et al., 2015; Kurachi et al., 2014). Importantly, studies to date narrowed the timing of BATF activity to somewhere within the first 3 days after $CD8^+$ T cell activation

Figure 6. KDM6B inhibition prior to first cell division impairs $CD8^+$ T cell expansion in response to activation

(A) Sort purified OT-I naive $CD44^{int/lo}$ $CD62L^{hi}$ $CD8^+$ T cells were either left untreated (mock) or treated with 10 μM of the J5 control and J4 inhibitor for 2 h in the presence of IL-2 before activating with the N4 peptide for 0, 1, 3, 5, and 24 h. Cells were then processed for ChIP-qPCR analysis for H3K27me3 and H3K4me3 at the promoters of *Tbx21*, *Irf4*, and *Irf8*. Data are representative of 2 independent repeats.

(B) The same samples were also used to assess transcriptional regulation of *Tbx21*, *Irf4*, *Irf8*, and *Tnf* using qPCR. Data shown are mean ± SEM from 3 independent repeats. Statistical significance was calculated using 2-way ANOVA (J4 versus mock and/or J5 control; *$p < 0.05$ **$p < 0.01$, ***$p < 0.001$).

(C) *In vivo* analysis of KDM6B inhibition on IAV-specific $CD8^+$ T cell responses. CTV-labeled OT-I $CD8^+$ T cells were untreated (mock) or treated with GSK-J5 or GSK-J4 for 4 h prior to adoptive transfer into C57BL/6 recipients, which were previously infected 3 days before with 10^4 plaque-forming unit (PFU) of X31-OVA. The proportion and number of $CD45.1^+/CD8^+$ OT-I T cells detected in the spleen (SPN), mediastinal lymph node (mLN), and the bronchoalveolar lavage (BAL) fluid were assessed by flow cytometry.

(D) The percentage and number of OT-I $CD45.1^+/CD8^+$ T cells undergoing a different number of cell divisions were assessed.

(E) Representative fluorescence-activated cell sorting (FACS) plot comparing the frequency of dividing OT-I $CD45.1^+/CD8^+$ T cells with mock, J5, or J4 treatment.

(F) The average number of cell divisions of $CD45.1^+$ OT-I $CD8^+$ T cells was compared between mock, J5, and J4 conditions. Data shown are mean ± SEM with 4–5 mice/group and are representative of 2 independent repeats. Statistical significance was calculated using a two-tailed Student's t test (*$p < 0.05$ **$p < 0.01$, ***$p < 0.001$).

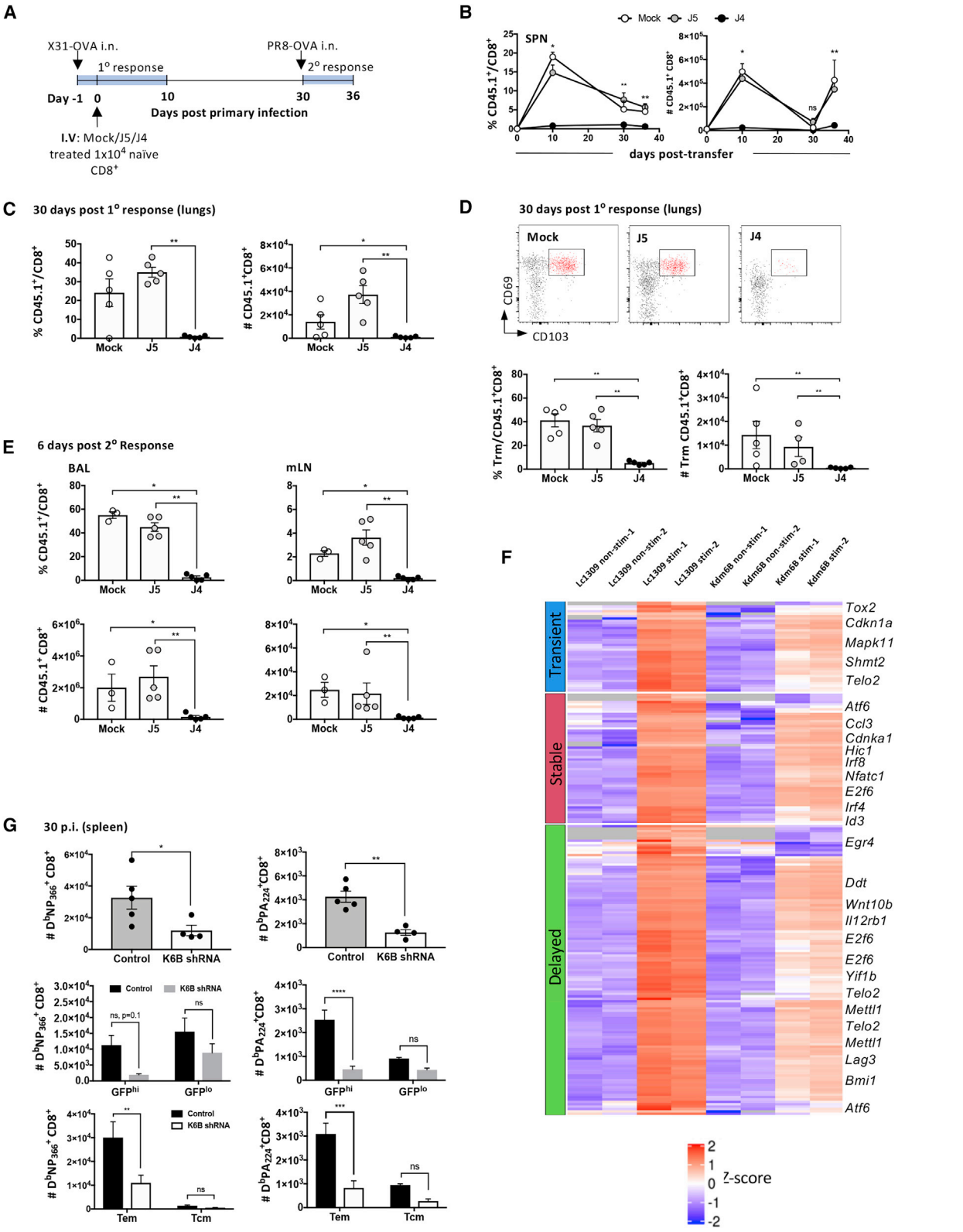

(legend on next page)

(Godec et al., 2015). Our data demonstrate that BATF activity is likely required in the very initial stages of T cell activation, and when paired with its binding partners (such as IRF4), it could potentially act as a pioneering factor helping remodel the chromatin landscape within hours of activation. Whether KDM6B recruitment is dependent on BATF or if H3K27me3 removal at target gene loci precedes BATF binding to initiate T cell activation will be of interest to examine in the future.

KDM6B-dependent removal of H3K27me3 was evident at the *Tbx21* locus as early as 3 h and stable up to 24 h after activation. This finding correlated with rapid upregulation of *Tbx21* transcription prior to cell division. T-BET upregulation was prior to the emergence of TBX21 binding sites within H3K27 demethylated regions found at 24 h after activation. We have recently shown that T-BET deficiency results in early dysregulation of virus-specific $CD8^+$ T cell differentiation that results in an inability to expand (Prier et al., 2019b). This was associated with decreased H3 acetylation at a T-BET target transcriptional enhancer within the *Ifng* locus. It has been previously demonstrated that T-BET can physically interact with and recruit H3K27 demethylases to the *Ifng* regulatory elements in $CD4^+$ T_H1 cells (Miller et al., 2008, 2010). Hence, we hypothesize that T-BET works downstream of pioneering factors, such as BATF/IRF4/RUNX3, by targeting $CD8^+$-T-cell-specific gene loci to further modulate chromatin remodeling. These results are reminiscent of a mechanism observed in stem cell differentiation in which early H3K27me3 removal, after receipt of differentiation signals, enables binding of lineage-specifying TFs to newly remodeled chromatin structures and commitment to a differentiated cell fate (Agger et al., 2007). Further analysis such as KDM6Bimmunoprecipitation to examine binding partners is something that could be explored in the future.

Inhibition of KDM6B activity prior to T cell activation had a profound impact on subsequent virus-specific $CD8^+$ T cell proliferation and the capacity to establish an effector memory T cell pool. Naive $CD8^+$ OT-I T cell treatment with the KDM6B inhibitor prior to adoptive transfer severely impacted the proliferative capacity of OT-I T cells responding to IAV infection. Despite the drug likely being diluted upon subsequent cell division, GSK-J4-treated OT-I $CD8^+$ T cells exhibited delayed division kinetics and failed to fully expand to levels observed in control-treated cells. This result suggests that early H3K27me3 removal is of critical importance for subsequent clonal expansion and differentiation. Concomitant with diminished proliferation in the lymph node, we observed that GSK-J4 OT-I $CD8^+$ T cells exhibited lower levels of T-BET expression and a lower proportion expressing multiple cytokines. These data further support the idea that molecular re-programming in the lymph node during the early stages of T cell activation is a key step for optimal effector T cell differentiation.

Deposition of H3K27me3 at key pro-memory genes has been reported to be important for the formation of optimal effector virus-specific T cell responses (Gray et al., 2017; Kakaradov et al., 2017). Limiting T cell proliferation has also been observed to promote the formation of memory $CD8^+$ T cell populations (Badovinac et al., 2004, 2005; Zehn et al., 2009). Hence, it was possible that inhibition of H3K27me3 removal would help promote memory formation. GSK-J4-treated OT-I $CD8^+$ T cells exhibited an intrinsic failure to expand upon secondary IAV challenge. In particular, we observed profound defects in the formation of lung-resident $CD8^+$ memory OT-Is (T_{RM}). Hence, KDM6B-dependent H3K27me3 demethylation during the early stages of a primary T cell response impacts efficient programming of both effector and memory $CD8^+$ T cell fates. The inability of GSK-J4-treated OT-I memory $CD8^+$ T cells to be recalled might reflect inappropriate installation of memory-associated H3K27me3 patterns. It would be of interest in the future to examine whether this memory dysfunction is associated with altered H3K27me3 patterns at memory-related gene loci. These data also suggest that commitment to effector and memory T cell fates are independent processes. This might reflect the role of distinct TFs. For example, we observed sequential unmasking of specific TF motifs for EOMES and RUNX3 TFs that have been shown to alter $CD8^+$ T cell differential potential for the formation of distinct memory T cell subsets (Mackay et al., 2015; Miller et al., 2008; Milner et al., 2017; Wang et al., 2018). By regulating the accessibility of these T cell lineage TF motifs during early hours of T cell activation, H3K27me3 demethylation therefore regulates the timely commitment to both effector and memory T cell fates.

Figure 7. Antigen-specific memory formation requires H3K27me3 removal during early $CD8^+$ T cell activation

(A) OT-I $CD8^+$ T cells either mock treated or treated with GSK-J5 or GSK-J4 for 4 h prior were adoptively transferred into C57BL/6 recipients infected with 10^4 PFU X31-OVA 1 day before (1° response). Mice were rested for 30 days before re-challenge with 10^4 PFU PR8-OVA (2° response).

(B) The proportion and number of $CD45.1^+CD8^+$ OT-I T cells were enumerated in the spleen of mice on day 10 and 30 post-transfer and again 6-days post-secondary challenge with PR8-OVA. These values were compared between the mock, J5, and J4 treatment. Data shown are mean ± SEM with 4–5 mice/group and are representative of 2 independent repeats.

(C) The proportion and the number of memory $CD45.1^+CD8^+$ OT-I T cells were enumerated in the lungs of mice 30-days post-primary infection with X31-OVA.

(D) Representative FACS plot of $CD45.1^+CD8^+$ resident memory T cells ($CD69^{hi}CD103^{hi}$) identified in the lungs mice that received $CD8^+$ OT-I T cells that received mock, GSK-J5, or GSK-J4 treatment. The proportion and number of mock-, GSK-J5-, or GSK-J4-treated $CD45.1^+CD8^+$ Trm cells were compared. Data shown are mean ± SEM with 4–5 mice/group and are representative of 2 independent repeats.

(E) The proportion and number of mock-, GSK-J5-, or GSK-J4-treated memory $CD45.1^+CD8^+$ OT-I T cells were enumerated in the BAL and mLN from mice that were challenged with PR8-OVA. Data shown are mean ± SEM with 4–5 mice/group and are representative of 2 independent repeats.

(F) The number of IAV-specific (D^bPA_{224} and D^bNP_{366}) $CD8^+$ T cells quantified in the spleen in VAV-tTA Lc1309 (control) and VAV-tTA *Kdm6b* shRNA mice 30 days post infection (d.p.i.) with 10^4 PFU X31. The number of IAV-specific $CD8^+$ T cells were compared between GFP (shRNA) high versus low cells between the control and *Kdm6b*-shRNA-expressing mouse strains. The number of IAV-specific T_{EM} and T_{CM} $CD8^+$ T cells were compared between the control and *Kdm6b*-shRNA-expressing mouse strains.

(G) RNA-seq analysis of non-stimulated and anti-CD3/28-stimulated $CD8^+$ T cells from *Kdm6b* and Lc1309 shRNA mice. Z scores are displayed for KDM6B-dependent genes with transient, stable, and delayed H3K27me3 demethylation. Data shown are mean ± SEM with 4–5 mice/group. All statistical significance shown here were calculated using a two-tailed Student's t test (*$p < 0.05$ **$p < 0.01$, ***$p < 0.001$).

STAR★METHODS

Detailed methods are provided in the online version of this paper and include the following:

- KEY RESOURCES TABLE
- RESOURCE AVAILABILITY
  - Lead contact
  - Materials availability
  - Data and code availability
- EXPERIMENTAL MODEL AND SUBJECT DETAILS
  - Animals
  - Primary Cell Cultures
- METHOD DETAILS
  - *In Vivo* Histone Demethylase Inhibition
  - Flow Cytometry
  - Total RNA extraction
  - RNA-sequencing
  - Chromatin Immuno-precipitation (ChIP) and Formaldehyde-assisted Isolation of Regulatory Element (FAIRE) Assays
  - ChIP-sequencing
  - ATAC-seq
  - Ciiider Analysis
- QUANTIFICATION AND STATISTICAL ANALYSIS

SUPPLEMENTAL INFORMATION

Supplemental Information can be found online at https://doi.org/10.1016/j.celrep.2021.108839.

ACKNOWLEDGMENTS

This work was supported by grants from the National Health and Medical Research Council of Australia (program grant 5671222 awarded to awarded to S.J.T. and N.L.L. and project grant APP1003131 awarded to S.J.T.) and an Australian Research Council Discovery grant (DP DP170102020 awarded to S.J.T. and S.R.); S.J.T. is supported by an NHMRC Principal Research Fellowship; and N.L.L. is supported by an Australian Research Council Future Fellowship. We thank the Monash Genomics Platform (Micromon) for high-throughput sequencing and the Monash Bioinformatics Platform for data analysis.

AUTHOR CONTRIBUTIONS

Conceptualization, S.J.T., J.L., and S.R.; methodology, J.L., K.H., M.O., L.J.G., X.Y.X.S., and A.B.; formal analysis, J.L., K.H., M.O., L.J.G., and X.Y.X.S.; investigation, J.L., J.E.P., X.Y.X.S., M.L.T.N., D.P., and B.E.R.; resources, S.J.T., S.R., and P.J.H.; data curation, K.H., M.O., and L.J.G.; writing – original draft, S.J.T. and J.L.; writing – review & editing, S.J.T., J.L., N.L.L.G., K.H., B.E.R., and S.R.; supervision, S.J.T.; acquisition of funding, S.J.T., P.J.H., N.L.L.G., and S.R.

DECLARATION OF INTERESTS

S.R. is currently the founder/chief scientific officer of EpiAxis Therapeutics. This manuscript received no funding from EpiAxis for this work. S.J.T. is a member of the scientific advisory board for Medicago, Inc., QC, Canada. This manuscript received no funding from Medicago for this work.

Received: February 26, 2020
Revised: November 24, 2020
Accepted: February 18, 2021
Published: March 16, 2021

REFERENCES

Agger, K., Cloos, P.A., Christensen, J., Pasini, D., Rose, S., Rappsilber, J., Issaeva, I., Canaani, E., Salcini, A.E., and Helin, K. (2007). UTX and JMJD3 are histone H3K27 demethylases involved in HOX gene regulation and development. Nature *449*, 731–734.

Araki, Y., Wang, Z., Zang, C., Wood, W.H., III, Schones, D., Cui, K., Roh, T.Y., Lhotsky, B., Wersto, R.P., Peng, W., et al. (2009). Genome-wide analysis of histone methylation reveals chromatin state-based regulation of gene transcription and function of memory CD8+ T cells. Immunity *30*, 912–925.

Badovinac, V.P., Porter, B.B., and Harty, J.T. (2004). CD8+ T cell contraction is controlled by early inflammation. Nat. Immunol. *5*, 809–817.

Badovinac, V.P., Messingham, K.A., Jabbari, A., Haring, J.S., and Harty, J.T. (2005). Accelerated CD8+ T-cell memory and prime-boost response after dendritic-cell vaccination. Nat. Med. *11*, 748–756.

Buenrostro, J.D., Wu, B., Chang, H.Y., and Greenleaf, W.J. (2015). ATAC-seq: A Method for Assaying Chromatin Accessibility Genome-Wide. Curr. Protoc Mol. Biol. *109*, 21.29.1–21.29.9.

Cao, R., Wang, L., Wang, H., Xia, L., Erdjument-Bromage, H., Tempst, P., Jones, R.S., and Zhang, Y. (2002). Role of histone H3 lysine 27 methylation in Polycomb-group silencing. Science *298*, 1039–1043.

Cook, K.D., Shpargel, K.B., Starmer, J., Whitfield-Larry, F., Conley, B., Allard, D.E., Rager, J.E., Fry, R.C., Davenport, M.L., Magnuson, T., et al. (2015). T Follicular Helper Cell-Dependent Clearance of a Persistent Virus Infection Requires T Cell Expression of the Histone Demethylase UTX. Immunity *43*, 703–714.

Cruz-Guilloty, F., Pipkin, M.E., Djuretic, I.M., Levanon, D., Lotem, J., Lichtenheld, M.G., Groner, Y., and Rao, A. (2009). Runx3 and T-box proteins cooperate to establish the transcriptional program of effector CTLs. J. Exp. Med. *206*, 51–59.

Denton, A.E., Russ, B.E., Doherty, P.C., Rao, S., and Turner, S.J. (2011). Differentiation-dependent functional and epigenetic landscapes for cytokine genes in virus-specific CD8+ T cells. Proc. Natl. Acad. Sci. USA *108*, 15306–15311.

Gearing, L.J., Cumming, H.E., Chapman, R., Finkel, A.M., Woodhouse, I.B., Luu, K., Gould, J.A., Forster, S.C., and Hertzog, P.J. (2019). CiiiDER: A tool for predicting and analysing transcription factor binding sites. PLoS One *14*, e0215495.

Godec, J., Cowley, G.S., Barnitz, R.A., Alkan, O., Root, D.E., Sharpe, A.H., and Haining, W.N. (2015). Inducible RNAi in vivo reveals that the transcription factor BATF is required to initiate but not maintain CD8+ T-cell effector differentiation. Proc. Natl. Acad. Sci. USA *112*, 512–517.

Gray, S.M., Amezquita, R.A., Guan, T., Kleinstein, S.H., and Kaech, S.M. (2017). Polycomb Repressive Complex 2-Mediated Chromatin Repression Guides Effector CD8^{+} T Cell Terminal Differentiation and Loss of Multipotency. Immunity *46*, 596–608.

Intlekofer, A.M., Takemoto, N., Wherry, E.J., Longworth, S.A., Northrup, J.T., Palanivel, V.R., Mullen, A.C., Gasink, C.R., Kaech, S.M., Miller, J.D., et al. (2005). Effector and memory CD8+ T cell fate coupled by T-bet and eomesodermin. Nat. Immunol. *6*, 1236–1244.

Intlekofer, A.M., Banerjee, A., Takemoto, N., Gordon, S.M., Dejong, C.S., Shin, H., Hunter, C.A., Wherry, E.J., Lindsten, T., and Reiner, S.L. (2008). Anomalous type 17 response to viral infection by CD8+ T cells lacking T-bet and eomesodermin. Science *321*, 408–411.

Jenkins, M.R., Webby, R., Doherty, P.C., and Turner, S.J. (2006). Addition of a prominent epitope affects influenza A virus-specific CD8+ T cell immunodominance hierarchies when antigen is limiting. J. Immunol. *177*, 2917–2925.

Jenkins, M.R., Kedzierska, K., Doherty, P.C., and Turner, S.J. (2007). Heterogeneity of effector phenotype for acute phase and memory influenza A virus-specific CTL. J. Immunol. *179*, 64–70.

Kaech, S.M., Hemby, S., Kersh, E., and Ahmed, R. (2002). Molecular and functional profiling of memory CD8 T cell differentiation. Cell *111*, 837–851.

Kägi, D., Ledermann, B., Bürki, K., Seiler, P., Odermatt, B., Olsen, K.J., Podack, E.R., Zinkernagel, R.M., and Hengartner, H. (1994). Cytotoxicity mediated by T cells and natural killer cells is greatly impaired in perforin-deficient mice. Nature *369*, 31–37.

Kakaradov, B., Arsenio, J., Widjaja, C.E., He, Z., Aigner, S., Metz, P.J., Yu, B., Wehrens, E.J., Lopez, J., Kim, S.H., et al. (2017). Early transcriptional and epigenetic regulation of CD8$^+$ T cell differentiation revealed by single-cell RNA sequencing. Nat. Immunol. *18*, 422–432.

Kallies, A., Xin, A., Belz, G.T., and Nutt, S.L. (2009). Blimp-1 transcription factor is required for the differentiation of effector CD8(+) T cells and memory responses. Immunity *31*, 283–295.

Kruidenier, L., Chung, C.W., Cheng, Z., Liddle, J., Che, K., Joberty, G., Bantscheff, M., Bountra, C., Bridges, A., Diallo, H., et al. (2012). A selective jumonji H3K27 demethylase inhibitor modulates the proinflammatory macrophage response. Nature *488*, 404–408.

Kurachi, M., Barnitz, R.A., Yosef, N., Odorizzi, P.M., Dilorio, M.A., Lemieux, M.E., Yates, K., Godec, J., Klatt, M.G., Regev, A., et al. (2014). The transcription factor BATF operates as an essential differentiation checkpoint in early effector CD8+ T cells. Nat. Immunol. *15*, 373–383.

La Gruta, N.L., Turner, S.J., and Doherty, P.C. (2004). Hierarchies in cytokine expression profiles for acute and resolving influenza virus-specific CD8+ T cell responses: correlation of cytokine profile and TCR avidity. J. Immunol. *172*, 5553–5560.

Lalvani, A., Brookes, R., Hambleton, S., Britton, W.J., Hill, A.V., and McMichael, A.J. (1997). Rapid effector function in CD8+ memory T cells. J. Exp. Med. *186*, 859–865.

LaMere, S.A., Thompson, R.C., Meng, X., Komori, H.K., Mark, A., and Salomon, D.R. (2017). H3K27 Methylation Dynamics during CD4 T Cell Activation: Regulation of JAK/STAT and IL12RB2 Expression by JMJD3. J. Immunol. *199*, 3158–3175.

Li, Q., Zou, J., Wang, M., Ding, X., Chepelev, I., Zhou, X., Zhao, W., Wei, G., Cui, J., Zhao, K., et al. (2014). Critical role of histone demethylase Jmjd3 in the regulation of CD4+ T-cell differentiation. Nat. Commun. *5*, 5780.

Liu, T., Ortiz, J.A., Taing, L., Meyer, C.A., Lee, B., Zhang, Y., Shin, H., Wong, S.S., Ma, J., Lei, Y., et al. (2011). Cistrome: an integrative platform for transcriptional regulation studies. Genome Biol. *12*, R83.

Mackay, L.K., Wynne-Jones, E., Freestone, D., Pellicci, D.G., Mielke, L.A., Newman, D.M., Braun, A., Masson, F., Kallies, A., Belz, G.T., and Carbone, F.R. (2015). T-box Transcription Factors Combine with the Cytokines TGF-β and IL-15 to Control Tissue-Resident Memory T Cell Fate. Immunity *43*, 1101–1111.

Miller, S.A., Huang, A.C., Miazgowicz, M.M., Brassil, M.M., and Weinmann, A.S. (2008). Coordinated but physically separable interaction with H3K27-demethylase and H3K4-methyltransferase activities are required for T-box protein-mediated activation of developmental gene expression. Genes Dev. *22*, 2980–2993.

Miller, S.A., Mohn, S.E., and Weinmann, A.S. (2010). Jmjd3 and UTX play a demethylase-independent role in chromatin remodeling to regulate T-box family member-dependent gene expression. Mol. Cell *40*, 594–605.

Milner, J.J., Toma, C., Yu, B., Zhang, K., Omilusik, K., Phan, A.T., Wang, D., Getzler, A.J., Nguyen, T., Crotty, S., et al. (2017). Runx3 programs CD8$^+$ T cell residency in non-lymphoid tissues and tumours. Nature *552*, 253–257.

Moffat, J.M., Gebhardt, T., Doherty, P.C., Turner, S.J., and Mintern, J.D. (2009). Granzyme A expression reveals distinct cytolytic CTL subsets following influenza A virus infection. Eur. J. Immunol. *39*, 1203–1210.

Northrop, J.K., Wells, A.D., and Shen, H. (2008). Cutting edge: chromatin remodeling as a molecular basis for the enhanced functionality of memory CD8 T cells. J. Immunol. *181*, 865–868.

Oehen, S., and Brduscha-Riem, K. (1998). Differentiation of naive CTL to effector and memory CTL: correlation of effector function with phenotype and cell division. J. Immunol. *161*, 5338–5346.

Pace, L., Goudot, C., Zueva, E., Gueguen, P., Burgdorf, N., Waterfall, J.J., Quivy, J.P., Almouzni, G., and Amigorena, S. (2018). The epigenetic control of stemness in CD8$^+$ T cell fate commitment. Science *359*, 177–186.

Peixoto, A., Evaristo, C., Munitic, I., Monteiro, M., Charbit, A., Rocha, B., and Veiga-Fernandes, H. (2007). CD8 single-cell gene coexpression reveals three different effector types present at distinct phases of the immune response. J. Exp. Med. *204*, 1193–1205.

Prier, J.E., Blewitt, M.E., Dickins, R.A., and Turner, S.J. (2019a). Development of a KDM6b shRNA conditional knock down mouse model. BioRxiv.

Prier, J.E., Li, J., Gearing, L.J., Olshansky, M., Sng, X.Y.X., Hertzog, P.J., and Turner, S.J. (2019b). Early T-BET Expression Ensures an Appropriate CD8$^+$ Lineage-Specific Transcriptional Landscape after Influenza A Virus Infection. J. Immunol. *203*, 1044–1054.

Rea, S., Eisenhaber, F., O'Carroll, D., Strahl, B.D., Sun, Z.W., Schmid, M., Opravil, S., Mechtler, K., Ponting, C.P., Allis, C.D., and Jenuwein, T. (2000). Regulation of chromatin structure by site-specific histone H3 methyltransferases. Nature *406*, 593–599.

Russ, B.E., Olshanksy, M., Smallwood, H.S., Li, J., Denton, A.E., Prier, J.E., Stock, A.T., Croom, H.A., Cullen, J.G., Nguyen, M.L., et al. (2014). Distinct epigenetic signatures delineate transcriptional programs during virus-specific CD8(+) T cell differentiation. Immunity *41*, 853–865.

Russ, B.E., Olshansky, M., Li, J., Nguyen, M.L.T., Gearing, L.J., Nguyen, T.H.O., Olson, M.R., McQuilton, H.A., Nüssing, S., Khoury, G., et al. (2017). Regulation of H3K4me3 at Transcriptional Enhancers Characterizes Acquisition of Virus-Specific CD8$^+$ T Cell-Lineage-Specific Function. Cell Rep. *21*, 3624–3636.

Scott-Browne, J.P., López-Moyado, I.F., Trifari, S., Wong, V., Chavez, L., Rao, A., and Pereira, R.M. (2016). Dynamic Changes in Chromatin Accessibility Occur in CD8$^+$ T Cells Responding to Viral Infection. Immunity *45*, 1327–1340.

Sen, D.R., Kaminski, J., Barnitz, R.A., Kurachi, M., Gerdemann, U., Yates, K.B., Tsao, H.W., Godec, J., LaFleur, M.W., Brown, F.D., et al. (2016). The epigenetic landscape of T cell exhaustion. Science *354*, 1165–1169.

van Stipdonk, M.J., Lemmens, E.E., and Schoenberger, S.P. (2001). Naïve CTLs require a single brief period of antigenic stimulation for clonal expansion and differentiation. Nat. Immunol. *2*, 423–429.

van Stipdonk, M.J., Hardenberg, G., Bijker, M.S., Lemmens, E.E., Droin, N.M., Green, D.R., and Schoenberger, S.P. (2003). Dynamic programming of CD8+ T lymphocyte responses. Nat. Immunol. *4*, 361–365.

Veiga-Fernandes, H., Walter, U., Bourgeois, C., McLean, A., and Rocha, B. (2000). Response of naïve and memory CD8+ T cells to antigen stimulation in vivo. Nat. Immunol. *1*, 47–53.

Wang, D., Diao, H., Getzler, A.J., Rogal, W., Frederick, M.A., Milner, J., Yu, B., Crotty, S., Goldrath, A.W., and Pipkin, M.E. (2018). The Transcription Factor Runx3 Establishes Chromatin Accessibility of cis-Regulatory Landscapes that Drive Memory Cytotoxic T Lymphocyte Formation. Immunity *48*, 659–674.e6.

Wei, G., Wei, L., Zhu, J., Zang, C., Hu-Li, J., Yao, Z., Cui, K., Kanno, Y., Roh, T.Y., Watford, W.T., et al. (2009). Global mapping of H3K4me3 and H3K27me3 reveals specificity and plasticity in lineage fate determination of differentiating CD4+ T cells. Immunity *30*, 155–167.

Xin, A., Masson, F., Liao, Y., Preston, S., Guan, T., Gloury, R., Olshansky, M., Lin, J.X., Li, P., Speed, T.P., et al. (2016). A molecular threshold for effector CD8(+) T cell differentiation controlled by transcription factors Blimp-1 and T-bet. Nat. Immunol. *17*, 422–432.

Yamada, T., Nabe, S., Toriyama, K., Suzuki, J., Inoue, K., Imai, Y., Shiraishi, A., Takenaka, K., Yasukawa, M., and Yamashita, M. (2019). Histone H3K27 Demethylase Negatively Controls the Memory Formation of Antigen-Stimulated CD8$^+$ T Cells. J. Immunol. *202*, 1088–1098.

Zediak, V.P., Johnnidis, J.B., Wherry, E.J., and Berger, S.L. (2011). Cutting edge: persistently open chromatin at effector gene loci in resting memory CD8+ T cells independent of transcriptional status. J. Immunol. *186*, 2705–2709.

Zehn, D., Lee, S.Y., and Bevan, M.J. (2009). Complete but curtailed T-cell response to very low-affinity antigen. Nature *458*, 211–214.

Zhang, Y., Liu, T., Meyer, C.A., Eeckhoute, J., Johnson, D.S., Bernstein, B.E., Nusbaum, C., Myers, R.M., Brown, M., Li, W., and Liu, X.S. (2008). Model-based analysis of ChIP-Seq (MACS). Genome Biol. *9*, R137.

Zhou, Y., Zhou, B., Pache, L., Chang, M., Khodabakhshi, A.H., Tanaseichuk, O., Benner, C., and Chanda, S.K. (2019). Metascape provides a biologist-oriented resource for the analysis of systems-level datasets. Nat. Commun. *10*, 1523.

STAR★METHODS

KEY RESOURCES TABLE

REAGENT or RESOURCE	SOURCE	IDENTIFIER
Antibodies		
anti-CD103 (2E7)	Biolegend	Cat# 121414; RRID:AB_1227502
anti-CD45.1 (A20)	BD Biosciences	Cat# 553776; RRID:AB_395044
anti-CD45.2 (104)	ebioscience	Cat# 17-0454-82;
anti-CD8 (53-6.7)	BD Biosciences	Cat# 563786; RRID:AB_469400
anti-CD44 (IM7)	ebioscience	Cat# 25-0441-82; RRID:AB_469623
anti-CD62L (MEL-14)	BD Biosciences	Cat# 104433; RRID:AB_394665
anti-IFNg (XMG1.2)	BD Biosciences	Cat# 554411; RRID:AB_395375
anti-IL2 (JES6-5H4)	Biolegend	Cat# 503808; RRID:AB_315302
anti-TNF (MP6-XT22)	Biolegend	Cat# 506308; RRID:AB_315429
anti-Va2 (B20.1)	BD Biosciences	Cat# 553288; RRID:AB_394759
anti-T-bet (eBio4B10)	ebioscience	Cat# 12-5825-82; RRID:AB_925761
anti-Gata3 (TWAJ)	ebioscience	Cat# 50-9966-42; RRID:AB_10596663
anti-B220 (RA3-6B2)	BD Biosciences	Cat# 553088; RRID:AB_394618
anti-F4/80 (BM8)	ebioscience	Cat# 11-4801-82; RRID:AB_2637191
anti-CD4 (GK1.5)	BD Biosciences	Cat# 553729; RRID:AB_395013
Bacterial and virus strains		
A/HKx31-OVA Influenza virus	Doherty Lab	https://doi.org/10.4049/jimmunol.177.5.2917; Jenkins et al., 2006
A/PR8-OVA Influenza virus	Doherty Lab	https://doi.org/10.4049/jimmunol.177.5.2917; Jenkins et al., 2006
A/HKx31	Doherty Lab	N/A
Chemicals, peptides, and recombinant proteins		
GSK-J4		N/A
GSK-J5		N/A
recombinant human IL-2		N/A
Ovalubumin 257-264 peptide (SIINFEKL)	AusPep	N/A
Influenza A nucleoprotein NP366-374 peptide (ASNENMETM)	AusPep	N/A
Influenza A acid polymerase peptide PA224-233 peptide (SSLENFRAYV)	AusPep	N/A
Critical commercial assays		
Fixation/Permeabilisation Solution Kit	BD Biosciences	Cat# 555028
FoxP3 Transcription Factor Staining Buffer Set	eBioscience	Cat# 00-5523-00
CellTrace Violet Cell Proliferation Kit	Life Technologies	Cat# C34557
NEBNext CHIP-seq Library Prep Master Mix Set for Illumina	New England BioLabs	Cat# NEB #E6240L,
Deposited data		
RNA-seq data: Activated OT-I T cell time course 0, 5 and 24 hr	This paper	Accession #: GSE166486. https://www.ncbi.nlm.nih.gov/geo/query/acc.cgi?acc=GSE166486
H3K27me3 ChIP seq data from *in vitro* activated OT-I T cells, 0, 5 and 24 hr.	This paper	Accession #: GSE166486. https://www.ncbi.nlm.nih.gov/geo/query/acc.cgi?acc=GSE166486

(*Continued on next page*)

Continued

REAGENT or RESOURCE	SOURCE	IDENTIFIER
ATAC-seq data Naive, or activated OT-I T cells at 3 and 24 hours after activation.	This paper	Accession #: GSE166486. https://www.ncbi.nlm.nih.gov/geo/query/acc.cgi?acc=GSE166486
RNA-seq data activated OT-I T cells 5h ± GSK-J4 KDM6B inhibitor	This paper	Accession #: GSE166486. https://www.ncbi.nlm.nih.gov/geo/query/acc.cgi?acc=GSE166486
RNA-seq and ChIP-seq data: naive effector memory CD8+ OTI T cells	Russ et al., 2014	Accession #: SRA: SRP049743; https://www.ncbi.nlm.nih.gov/sra/?term=SRP049743
Experimental models: organisms/strains		
OT-I Transgenic mouse strain		RRID:IMSR_JAX:003831
C57BL/6J		RRID:IMSR_JAX:000664
Vav-Tta K6B shRNA		DOI:, (Prier et al., 2019a), generated in house
Vav-Tta Lc1309 shRNA		DOI:, (Prier et al., 2019a), generated in house
Oligonucleotides		
Irf4_Promoter_F_CTGTAGTCGGGCAGAAGGAG	Integrated DNA Technologies	N/A
Irf4_Promoter_R_GGTCCGCTATCTCAGCATTC	Integrated DNA Technologies	N/A
Irf8_Promoter_F_AGAGGCTCTCCAAACCTGAAC	Integrated DNA Technologies	N/A
Irf8_Promoter_R_TCCGAGAAATCACTTTTGCAC	Integrated DNA Technologies	N/A
Tnf_Promoter_F_GTAGGGCCACTACCGCTTC	Integrated DNA Technologies	N/A
Tnf_Promoter_R_AGACGGCCGCCTTTATAGC	Integrated DNA Technologies	N/A
Tbx21_Promoter_F_GAATTCGCGCTGTATTAGCC	Integrated DNA Technologies	N/A
Tbx21_Promoter_R_GCCTTTGCTGTGGCTTTATG	Integrated DNA Technologies	N/A
Irf4_Taqman gene expression probe	Life Technologies	Assay ID: Mm00516431_m1
Irf8_Taqman gene expression probe	Life Technologies	Assay ID: Mm00492567_m1
Tnf_Taqman gene expression probe	Life Technologies	Assay ID: Mm00443258_m1
Tbx21_Taqman gene expression probe	Life Technologies	Assay ID: Mm00450960_m1
Kdm1b_Taqman gene expression probe	Life Technologies	Assay ID: Mm00552098_m1
Kdm3b_Taqman gene expression probe	Life Technologies	Assay ID: Mm00804683_m1
Kdm5b_Taqman gene expression probe	Life Technologies	Assay ID: Mm03053411_s1
Kdm6b_Taqman gene expression	Life Technologies	Assay ID: Mm01332680_m1
Kdm6a_Taqman gene expression	Life Technologies	Assay ID: Mm00801998_m1
L32_Taqman gene expression	Life Technologies	Assay ID: Mm00777741_sH
Software and algorithms		
Homer	http://homer.ucsd.edu/homer/	RRDI:SCR_010881
Cistrome	http://cistrome.org/	RRDI:SCR_005396
Bedtools	https://bedtools.readthedocs.io/en/latest/	RRDI:SCR_006646
Metascape		RRDI:SCR_016620
ggplot2	https://cran.r-project.org/web/packages/ggplot2/index.html	RRDI:SCR_014601
Macs2		RRDI:SCR_013291
R	https://cran.r-project.org/	RRDI:SCR_001905
Deeptools		RRDI:SCR_016366
DAVID	https://david.ncifcrf.gov/	RRDI:SCR_001881
Ensembl		RRDI:SCR_002344
Biomart		RRDI:SCR_010714
FlowJo vs9 and 10	FlowJo	RRID:SCR_008520
Prism vs7	GraphPad	RRID:SCR_005375

RESOURCE AVAILABILITY

Lead contact

Further information and requests for resources and reagents should be directed to and will be fulfilled by the corresponding author, Professor Stephen Turner (stephen.j.turner@monash.edu).

Materials availability

The shRNA transgenic mice for *Kdma6b* knockdown (*shKDM6b*) have been previously described (Prier et al., 2019a). These mice and appropriate controls are available contingent on signing of appropriate Material Transfer Agreements between Institutions. All other materials are freely available.

Data and code availability

All genomic data (H3K27me3 ChIP-seq; RNA-seq) data has been deposited into the Gene Expression Omnibus (GEO) database. Accession number is: GSE166486

EXPERIMENTAL MODEL AND SUBJECT DETAILS

Animals

For *in vitro* studies, male, C57BL/6-Tg(TcraTcrb)1100Mjb/J (also known as OT-I mice) of 6-8 weeks of age were utilized. These mice contain transgenes encoding for T cell receptor chains (TRAV14 and TRBV12-1) specific for the H2-K^b binding ovalbumin peptide ($OVA_{257-264}$; SIINFEKL amino acid sequence). For adoptive transfer studies, female or male CD45.2^+ OT-I $CD8^+$ T cells were adoptively transferred into sex matched CD45.1 mice (B6.SJL-*Ptprc*^{a} *Pepc*^{b}/BoyJ). For shRNA studies, male and female $KDM6b^{shRNA}$ transgenic mice (C57BL/6J, 6-8 weeks) were utilized. $KDM6b^{shRNA}$ mice were crossed onto C57BL/6J mice that were transgenic for the tetracycline transactivator protein, under the control of the CMV promoter (CMV-rtTA) to generate $KDM6b^{shRNA}$ x CMV-rtTA mice. As controls, transgenic mice encoding the shRNA for luciferase (C57BL/6J-Luc^{shRNA}) were used for crosses onto CMV-rtTA transgenic line. All mice were housed in specific-pathogen free conditions at the Monash Animal Research Platform. Housing and experimental procedures were approved by the Monash University Animal Ethics Committee.

Primary Cell Cultures

Naive OT-I $CD8^+CD44^{lo/int}$ cells were purified from OT-I/Ly5.1 male mice (6-8 weeks) (> 99% purity). They were stimulated with 1 μM OVA (N4) for 0, 1, 3, 5 and 24 hours at the presence of rhIL-2 (10U/mL) in complete RPMI supplemented with 10% heat-inactivated fetal calf serum, 2mM L-glutamine, 1mM MEM sodium pyruvate, 100 μM MEM non-essential amino acids, 5mM HEPES, 55 μM mercaptoethanol, 100U/mL penicillin and streptomycin. For demethylase inhibition, purified OT-I $CD8^+$ T cells were pre-treated with 10 μM of the control inhibitor (J5) or the Kdm6b inhibitor (J4) for 2hrs in complete RPMI with rhIL-2 (10U/mL) before stimulation with the N4 peptide for 0, 1, 3, 5 and 24 hours.

METHOD DETAILS

In Vivo Histone Demethylase Inhibition

Total lymph nodes were extracted from OT-I females (6-10 weeks). They were resuspended to generate a single cell suspension followed by labeling with the CellTrace Violet Cell Proliferation kit. A total of $4x10^6$ lymphocytes were used for either the mock treatment or pretreatment with either the substrate specificity control (J5) or the H3K27me3 demethylase inhibitor (J4) in rhIL-2 (10U/mL) for 4hrs. A portion of these cells were used to stain with the Annexin V kit with PI and anti-CD44-PE-Cy7, CD62L-BV570, CD8-APC and CD45.1-PE antibodies. A proportion of $3x10^5$ naive ($CD44^{int/lo}CD62L^{hi}$) $CD8^+$ cells were then intravenously injected into female C57BL/6 mice (6-8 weeks) that had been infected with 10^4 pfu HKx31-OVA (Jenkins et al., 2006) for 3 days (early time point) or 10^4 naive ($CD44^{int/lo}CD62L^{hi}$) $CD8^+$ cells were used for determining early memory formation at day 30 post-infection. At these time points, the spleen (SPN), mediastinal lymph nodes (mLN) and bronchoalvelolar lavage (BAL) fluid or the lungs were extracted to prepare for single cell suspension.

Flow Cytometry

Single cell suspension from spleen or lymph nodes were blocked with 2.4G2, anti-rat and anti-mouse serum on ice for 15 mins before they were centrifuged (1600rpm, 5mins). After discarding the supernatant, cells were stained with LIVE/DEAD™ Fixable Aqua Dead Cell Stain (Thermo Fischer Scientific) for 10 mins at room temperature. Cells were washed with MACS buffer (2mM EDTA, 2% BSA in PBS) followed by re-suspension in antibody cocktail containing various mixtures of fluorochrome conjugated antibodies specific for CD4, CD8, CD45.1, CD45.2, CD44, CD62L, Klrg1, CD127, CD69 and CD103. For cytokine staining, cells were permeabilised according to manufacturer's instructions (BD Biosciences) followed by staining with anti-IL-2, TNF and IFN antibodies. For intranuclear transcription factor staining, cells were permeabilised according to manufacturer's instructions (eBioscience). Stained cells were washed twice with either permeabilization buffer and MACS buffer for cytometry analysis. Samples were acquired on then FACSCanto II or

the Fortessa flow cytometers (BD Biosciences) coupled to the high through system (HTS). Post-acquisition data analyses were performed using FlowJo software (Tree Star, Ashland, OR, USA). Mean fluorescence intensity (MFI) or the frequency (%) of staining was determined for the population of interest.

Total RNA extraction

Total RNA was extracted using Trizol® from unstimulated or stimulated OT-I CD8$^+$ T cells. For gene expression analysis, 100 μg mRNA was converted to cDNA using the Omniscript kit (Invitrogen) according to manufacturer's instructions. Relative gene expression changes were determined by quantitative real time-PCR using the CFX-Connect Real-Time System (Biorad) with Taqman ® Gene MGB primer/probes (Life Technologies).

RNA-sequencing

RNA samples (triplicates) were depleted of DNA and purified using the QIAGEN RNeasy MinElute kit. The bioanalyzer was used to determine the integrity of the RNA before library preparation using the kit. RNA libraries were sequenced paired end (100bp) on the Hiseq2000 instrument at the Australian Genome Research Facility, the Walter and Eliza Hall Institute of Medical Research, Melbourne, Australia. Data quality was confirmed with fastqc software. Paired end RNA-seq data was mapped to mouse genome mm10 using TopHat (with Bowtie2). Only concordant pairs with mapping quality greater than 10 were utilized. Reads were assigned to annotated genes using Feature Counts from R subread Bioconductor R package. Genes which did not have at least 3 counts in each sample in at least one group were excluded from the analysis. Differential Expression analysis was done using edgeR Bioconductor R package. Genes were considered DE if exhibited FDR < 0.05 and log2 FC > 1. Log averages of the triplicates for the differential genes were clustered using Manhattan distance, complete linkage (R) and grouped using the z-score of the averaged TMM normalized values (EdgeR) with K means (R).

Chromatin Immuno-precipitation (ChIP) and Formaldehyde-assisted Isolation of Regulatory Element (FAIRE) Assays

Cells crosslinked with 0.6% formaldehyde were sonicated and immune-precipitated with anti-H3K4me3 and H3K27me3 ChIP-grade antibodies and Protein A magnetic beads (Millipore). Total input and no-antibody control for each sample was included for normalization and specificity control purposes. Immuno-precipitated DNA was purified and re-suspended in 0.1X TE buffer. For FAIRE-analysis, open chromatin was extracted twice by adding an equal volume of phenol:chloroform:isoamyl (25:24:1) (Sigma) and precipitated as described for ChIP assays. Resulting ChIP or FAIRE-DNA was compared using quantitative real time-PCR on the CFX-Connect Real-Time System (Biorad) with Sybr-green master mix using primers spanning region of interest. Real-time PCR cycle threshold (Ct) values were converted to copy number and background immunoprecipitation subtracted (no-antibody control).

ChIP-sequencing

ChIP-DNA was prepared for sequencing using the NEBNext® CHIP-seq Library Prep Master Mix Set for Illumina (NEB #E6240L, New England BioLabs Inc) according to manufacturer's instructions. ChIP-DNA library was subjected to size selection with AMPure beads. The quality of the ChIP-DNA library and the fragment size of approximately 275 bp were assessed on the Bioanalyzer using the Agilent High Sensitivity DNA chip (Agilent Technologies, 5067-4626). ChIP libraries were sequenced paired end on the Hiseq2500 instrument at the Australian Genome Research Facility (AGRF). Differential ChIP-seq peaks were found by creating windows of counts (bigwig files normalized per 10 million reads (HOMER)) for each treatment, finding the differences between windowed counts (DeepTools) and then calling peaks in MACS2 (bdgpeakcall -c 3 -l 150 -g 300) (Zhang et al., 2008). Regions were intersected using Bedtools and annotated using HOMER, CISTROME (Liu et al., 2011) (in conjunction with BedTools) and transcription start sites taken from ENSEMBL. DAVID and Metascape (Zhou et al., 2019) were used to examine gene groups for enriched Gene Ontology terms.

ATAC-seq

ATAC-seq is adapted from Buenrostro et al. (2015). A total of 50 000 cells were lysed with cold lysis buffer for nuclei extraction. Nuclei were immediately resuspended in transposition reaction mix prepared from the Illumina Nextera DNA Sample Preparation Kit (FC-121-1030) for 30 minutes at 37°C. Transposed DNA was extracted using the QIAGEN MinElute PCR Purification kit (Cat #. 28004). Resulting DNA was subjected to 5 PCR cycles on the thermocycler using a PCR primer 1 (Ad1_noMX) and an indexed PCR primer 2. An aliquot of each sample was used subsequently in a real-time quantitative PCR for 20 cycles to determine the number of cycles required for library amplification. The amplified DNA was purified using the QIAGEN MinElute PCR Purification kit. Library quality was assessed using the bioanalyzer (Agilent) to ensure that the DNA fragmentation ranges between 50-200bp and the Qubit to determine the overall DNA concentration. ATAC-DNA was sequenced paired end on the Hiseq2500 instrument at the Australian Genome Research Facility (AGRF).

Ciiider Analysis

CiiiDER analyisis was carried out according to Gearing et al. (2019) and Russ et al. (2017). Briefly, peaks with a length greater than 400 were filtered out. Regions of equal size were defined from 200 bases upstream to 200 bases downstream of the middle of each peak using the Mus_musculus.GRCm38.dna.primary assembly.fa genome. CiiiDER analysis was performed on these regions with JASPAR_CORE_vertebrates_2016.txt transcription factor position frequency matrices and a deficit cut-off of 0.15.

QUANTIFICATION AND STATISTICAL ANALYSIS

In Figure 1, RNaseq and gene expression data are shown as fold change (log2) or mean ± SEM from 3 independent repeats with statistical significance calculated using a one-tailed Student's t test (*$p < 0.05$ **$p < 0.01$, ***$p < 0.001$) as indicated in the figure legend. In Figures 2, 3, and 4, H3K27me3 ChIP-seq, CISTROME and their statistical analysis are detailed in the main text and figure legends. Figures 5 and 6, flow cytometry data shown are mean ± SEM with 4-5 mice/group and are representative of 2-3 independent repeats. Statistical significance calculated using a two-tailed Student's t test (*$p < 0.05$ **$p < 0.01$, ***$p < 0.001$). Statistical tests used are shown in each of the figure legends.